Lessons from structural analysis of a great Gothic cathedral: Canterbury cathedral as a case study

Georgios Karanikoloudis, Paulo B. Lourenço, Leslie E. Alejo*, Nuno Mendes

ISISE, Department of Civil Engineering, University of Minho, Guimarães, Portugal

* Correspondence to Leslie E. Alejo, ISISE, Department of Civil Engineering, University of Minho, Campus de Azurém, Guimarães, 4800-058, Portugal; E-mail: leslie.alejoguerra@gmail.com; Tel: +351 253 510 20078

Lessons from structural analysis of a great Gothic cathedral: Canterbury Cathedral as a case study

Damage in Gothic cathedrals can occur due to single extreme events or long term processes, often associated to large deformations and cracking. This paper, presents the damage survey and structural assessment of a UNESCO world heritage site and one of the oldest, most visited and most known Christian temples in the UK: Canterbury Cathedral, in Kent. Inspection and damage survey showed repetitive crack patterns on the vault's intrados, with more severity in the south aisle, including namely outward rotating movement and cracking in the south flying buttresses. Ambient vibration tests were carried out to identify the structure modal properties. A FE model of a typical transversal section of the nave and lateral aisles was prepared, and calibrated based on the tests. Nonlinear static analyses were performed, considering the main parameters of influence to the structure, as the construction process, the infill volume, the presence of lateral thrusts from the nave's roof and differential settlements. A validated FE model, presenting sufficient correlation with the existing damage was used to determine the safety factors for lateral and vertical loading, which according to the local hazard are considered adequate. A comparison with limit analysis, based in the static approach, was also carried out.

Keywords: English Gothic Architecture; Nonlinear Structural Analysis; Damage Survey; Safety Analysis; Phased Analysis; Graphic Statics.

Research aims:

- To identify the types of damage affecting the building through inspection and damage survey;
- To provide basis for discussion on structural behaviour of Gothic cathedrals ;
- To understand the cause of the existing damage by analysing different hypothesis (self-weight loading, construction process, soil settlements);
- To assess the safety of the structure.

1 Introduction

The evaluation of the structural performance and damage in cultural heritage buildings requires a methodology that involves namely advanced numerical methods, monitoring, historic research and inspection. Damage in Gothic cathedrals is mostly related to large deformations and cracking due to tensile failure of masonry. As deformation increases, the structure exhibits fragmentation and rotations in the arches and vaults, caused by tensile damage. Cracks due to compressive stresses can also propagate in localized areas, manifesting namely as vertical cracks in columns as well as spalling of ribs and capitals. Creep phenomena are also relevant for crack propagation and can occur even under moderate compressive stresses (Roca et al. 2008; Roca and Clemente 2005). Cyclic environmental effects (e.g. due to temperature effects or water table level in the ground) also contribute to damage progress.

Material deterioration can also affect the mechanical and physical properties of structural elements, either from long term environmental influence (freeze-thaw cycles, thermal effects, corrosive agents, moisture infiltration, salts efflorescence, etc.) or from short term events (fires, floods, etc.). The magnitude of the actions and condition of the building can determine if the structure is affected at a local or global scale (Roca and Clemente 2005).

Other relevant influence factors are associated with the construction process, such as alterations and reconstructions, as they cause extensive damage in historical constructions. Overall instability and differential settlements can be caused by the addition of new parts, many of which were not considered in the initial design. In general, Gothic cathedrals had many construction periods, sometimes lasting decades, with subsequent alterations and demolitions, during which many deformations occurred due to the lack or early removal of supports, lateral confinements and bracing (Roca and

Clemente 2005). The most common additions were the erection of new towers and the extension of existing ones, such as in the central crossing tower in Wells Cathedral, UK, causing the tower's westward leaning (D'Ayala and Smars 2003). Moreover, many structural interventions, such as reinforced concrete beams and ties, often introduced excessive or eccentric loading, changing the past structural behaviour. These additions, during extreme dynamic conditions, can even cause sudden failures (D'Ayala and Smars 2003).

Accidental actions were the cause of immense damage in many Gothic cathedrals, especially from blast waves or even direct hits from shelling during the warfare combats, such as Rheims Cathedral in France, struck by German shellfire in 1915 (Theodossopoulos and Sinha 2008). Recently, the case of Notre-Dame Cathedral (Paris) showed how fire can be responsible for vast damage on heritage buildings. The fire, located in the main roof, started on 15th April 2019 and triggered the collapse of the last bay in the north transept, one bay in the nave, and likewise, the square vault at the crossing as a collateral damage due to the collapse of the oak spire over it (Heyman 2019; Ferreira 2019).

Regarding seismic loading, failure modes in Gothic cathedrals typically consist of separation of large rigid elements that experience out of plane rotation. This type of kinematic mechanisms can involve the rotation of whole facades and towers, or parts of them. But under specific ground excitations, the most critical failure modes can be identified (Roca et al. 2010). Visual inspections and damage surveys can determine the level of damage in masonry. The evaluation of deformations and cracks, and mainly their evolution along time, is very important for diagnosis of the structure, since it can be used to identify structural and non-structural damage, active and non-active damage, and failure mechanisms in case of an extreme event (Ramos and Lourenço 2014). A Gothic cross vault can experience cracks parallel to the direction of the side walls, known as Sabouret's cracks, caused by high levels of stiffness in confined spans. In the case of an outward movement of the supports, the failure mechanism consists of four hinges: one in each springing (extrados), and two in the proximity of the crown (intrados) (Theodossopoulos 2008). Due to the vulnerability and the relevance of such structural systems, several studies on performance of cross vaults, based on lab scaled tests and nonlinear numerical analyses (Carfagnini et al. 2018; Gaetani et al. 2017; Gaetani et al. 2016).

In situ measurements, such as dynamic identification tests, sonic tests and flat jack tests, provide confidence in the simulation of the actual structural response (Roca et al. 2010; Roca and Clemente 2005). In particular, dynamic identification tests are considered an efficient tool for the calibration of the mechanical and physical parameters of numerical models in linear range, such as the linear stiffness (Ramos 2007).

The current study, started with the concern about cracks observed at the aisles of the Canterbury cathedral. As a result, a multidisciplinary approach was followed in order to assess the structural performance. Thus, the University of Minho, invited by the Morton Partnership (company of Consulting Structural Engineers), carried out a research on the damage and structural performance of the aisle. Through hypotheses defined from the historic investigation and the in situ damage identification, FE models were built and analysed with the initial aim of reproducing the actual state of the building.

The geometrical model of the transverse cross section with its corresponding bay, was used for the 3D FE model. The discretized structural elements were composed of homogeneous masonry materials, for which cracking and crushing were described with nonlinear relationship incorporating softening, based on the fracture energy concept (Lourenço 1998).

Assuming that the documented structural damage was mostly the result of cumulative phenomena, various nonlinear numerical analyses assessed the building's capacity to sustain self-loads, lateral effects, foundation settlements and excessive lateral thrusts from the roof trusses and infill volumes. In the modelling process, various assumptions were incorporated and the construction process was also simulated. The adopted strategy of damage identification, structural assessment and understanding obtained here is of value for Gothic cathedrals in general.

2 History of Canterbury cathedral

Canterbury cathedral is one the most prestigious and prominent ecclesiastic structures in UK (**Erro! A origem da referência não foi encontrada.**). It is the seat of the Archbishop of Canterbury, head of the Anglican Church and an established UNESCO World Heritage site since 1988. After a long sequence of construction phases, the cathedral is a mixture of Romanesque, Early Gothic, Decorated Gothic styles and following interventions, dated from 1070 to 1834 (Collinson, Ramsay, and Sparks 1995).

St Augustine, arrived in Kent from Rome in 597, was consecrated the first Archbishop of Canterbury and established the first cathedral, located in a north-east part of the city. Until 1070 the cathedral evolves under four specific phases: (I) The original church consisted of a simple nave and an apsidal altar, surrounded along the west, north and south sides by porches; (II) The cathedral comprises partly additions on the previous church and of a baptistery-church and mausoleum for the Archbishops, near the south-east corner of the nave (740-760); (III) During the 9^{th} or 10^{th} century a massive enlargement of the cathedral takes place, involving the widening of the foundations. The porches were incorporated into side-aisles and the cathedral doubles in length (then to 49m by 23m). The whole process was a part a reorganization of the site to include monastic buildings; (IV) The squared west front of the cathedral is demolished and replaced with a major west polygonal apse, making the cathedral bipolar. Flanking hexagonal stair towers were built in the west front, the arcade walls were strengthened and two towers were added at the eastern corners. From the excavated remains of Phase IV, as seen in **Erro! A origem da referência não foi encontrada.**a, the cathedral was 75m in length and 31m in width. The monastic complex, along with the church, was burnt by a great fire in 1067 (Collinson, Ramsay, and Sparks 1995).

The successor Norman Cathedral in 1070 had one transept and a tower at its crossing, with a steeple terminated by a golden angel. The nave was arranged in eight bays and on the west front two twin towers were raised, terminated with gilded pinnacles (the cathedral of Lanfranc, as seen in **Erro! A origem da referência não foi encontrada.**b). In 1096, Archbishop Anselm, demolished the Choir and the underground crypts. The new choir extended 58m from the crossing to the east and included an ambulatory passage with chevette chapels, new altars in three levels and an attaching chapel of the Holy Trinity (**Erro! A origem da referência não foi encontrada.**c, **Erro! A origem da referência não foi encontrada.**e). The new Choir was destroyed in 1174 by fire and was reconstructed by William of Sens and increased in he ight by 3.7 m. The implementation of the new Choir was taken over by William the Englishman, who incorporated the transition from the Romanesque to the Gothic style (**Erro! A origem da referência não foi encontrada.**d, **Erro! A origem da referência não foi encontrada.**e) (Collinson, Ramsay, and Sparks 1995).

In 1378 Archbishop Sudbury started the demolition and total rebuilding of Lanfranc’s nave, accounting for its bad state, but the attempt was terminated because of his death in 1381. An earthquake in 1382 damaged severely the Cathedral’s bell tower and cloister. The reconstruction of the nave and transepts in the Perpendicular English

Gothic style was later on assigned to Prior Thomas Chillenden (1391-1411). All piers were replaced with slender ones, while the side walls in the aisles were demolished and rebuilt. The vaults were constructed as lierne vaults with bosses and the nave roof was raised, so as to align with the choir roof. The south-west tower was replaced in 1459. The square tower at the crossing was demolished in 1430 and its supporting piers were reinforced, so as to support the new bigger one, which was completed in 1504 at its complete height of more than 70m. The north-west tower was demolished in 1834 due to structural deficiencies and replaced with a twin of the south-west tower. The north-west tower's spire was maintained until 1705 (Collinson, Ramsay, and Sparks 1995; Willis 1845).

3 20th century's intervention & conservation works

During World War II the city of Canterbury was severely bombarded, which led to the bond weakening and separation of the outer masonry layer. In an attempt to re-establish its former condition, the masonry exterior walls were grouted using a strong Portland cement, which accelerated the stonework's decay and changed the moisture migration. In repairing works at the central tower and pinnacles, Bath stone was used, which is incompatible with the original Caen stone, as being more coarse and grainy in texture and darker in colour (Foyle, Greshoff, and Newton 2013; Canterbury Cathedral 2014).

After 1970s, a good quality limestone from the south west of France, known as Lepine, was chosen for repairing works, given that Caen stone was hard to find in the desired quantity or quality. Several projects were carried out: (a) Reconstruction of the gable at the south west transept, with a reinforced concrete cantilever beam, connecting the gable with the rest of the building; (b) Conservation of the south window's glass panels; (c) Large scale repairs in the cathedral's west end, rebuilding of the oculus and gable and stone replacements at the twin towers of the west front (Foyle, Greshoff, and Newton 2013; Canterbury Cathedral 2013; Filippoupolitis 2011).

After 1990s, the floor in the cathedral's nave and south west transept was replaced with a Portland concrete slab floor laid over a lime screed, together with an under-floor heating system. As a fire resistance strategy, soon after the fire in the roof of York Minster Cathedral in 1984, a concrete layer was added in the infill of the aisles and nave, serving as an impermeable surface to drain more effectively the amount of water used to extinguish a potential fire, through drilled holes in the lateral walls (Canterbury Cathedral 2013).

From 2009 to 2012 a conservation project of the South East Transept took place. The stained glass panels from the South Oculus were removed and treated. The wrought iron frame called 'ferramenta', which supports the stained glass window and dates from 1180, underwent mechanical cleaning for rust removal and wax coating, with rust inhibitors applied. Additionally, the timber roof of the South East Transept, being the oldest part of the Cathedral's roof system, underwent timber repairs and replacement of its lead tiles covering, while the exterior wall cladding was treated for black crust removal and replacement of cement with lime mortar (Canterbury Cathedral 2011; ACNS 2007). A monitoring system was installed in 2010, gathering information on temperature, relative humidity and displacements in the roof spaces, ground floor, crypt, Bell's Harry interior, south west transept and flying buttresses on the south side of the nave. Crack-meters and tilt-meters installed at some of the flying buttresses and at clerestory walls, respectively, provided data on deformations occurred at zones considered in this work (**Erro! A origem da referência não foi encontrada.**). From 2006 to 2012, works in the Corona Chapel accounted for the stone masonry and stained glass windows conservation (Canterbury Cathedral 2012).

The Great South Window of the South West Transept tracery experienced cracks and fracturing, due to embedded iron rusted bars and outward tilting. All the stained window panels have been removed and the tracery was repaired in all its extent by stone replacements (Canterbury Cathedral 2014).

In September 2016, a big project of conservation for Canterbury Cathedral was successfully granted by the Heritage Lottery Fund (HLF 2018, 88). Concerning conservation, three main objectives were defined: a) the repair and restoration of the Christ Church Gate; b) the repair and restoration of the West Towers and Nave Roof; c) the improvement of the access and Landscape South Precincts (Canterbury Cathedral 2017). The work continues until this moment, and it is expected to be finished by the end of 2021 (Canterbury Cathedral 2019a). In the meanwhile, at the beginning of 2019, founded by the Viridor Credits Environmental Company, repair works started to restore the South Quire Tribune roof and the Quire gutters (Canterbury Cathedral 2019b).

4 Geometrical survey

The in situ geometrical survey, carried out by Downland Partnership Ltd and provided by the Morton Partnership Ltd, focused on the central nave, the adjoining lateral aisles and the attaching cloister in the north, as shown in **Erro! A origem da referência não foi encontrada.**. The collected information resulted in digitalized details, such as the section of pillars, the cross section of the nave in the area of interest and the external elevation of the typical bay.

The nave, with overall dimensions of 48.6 m in length, 10.5 m in width and 24.6 m of inner height, is organised in 8 bays, covered with Gothic lierne quadripartite cross vaults and equilateral pointed arches (**Erro! A origem da referência não foi encontrada.**a-c). The vaults have a clear span of 9.4 m and 5.2 m in the transverse and longitudinal direction and a rise of 6.3 m. The thickness of the nave vault, measured from a cylindrical void in a boss, is 0.8 m, accounting the portion of the boss (protrusion of stone) and the intersecting diagonal ribs that project below the web of the vault. Thus, the design shell thickness of the vaults was accounted as 0.4m and considered constant. The ribs are considered an essential part of the vault's structural system, providing safe enclosure of the web masonry (Theodossopoulos 2006). Nevertheless, due to the limited information on their size and configuration and aiming at simplifying the geometry of the 3D CAD and FE model, the diagonal and transversal ribs were not taken into account for the model. Adjacent equilateral pointed nave arches of 4.0 m clear span, 5.4 m rise and 0.9 m width are the structural elements of the clerestory walls (**Erro! A origem da referência não foi encontrada.**d).

The lateral aisles comprise 8 bays with dimensions 6.6 x 5.9 m and 15.1 m in height. The cross vaults are Gothic lierne quadripartite, drawn from equilateral pointed arches. The adjacent arcade arches have a clear span of 4.0 m, 3.5 m rise and 0.9 m width, whereas the arches of the aisles windows have a clear span of 2.9 m, with 2.9 m rise and 1.4 m width. The thickness of the vaults in the lateral aisles was considered equal to the thickness of the nave, i.e. 0.4 m (**Erro! A origem da referência não foi encontrada.**e).

The vertical abutments in the nave consist of a colonnade of 7 piers on both sides, with the level of springings of the nave and lateral vaults at 18.3 m and 11 m respectively. The piers section has an area of 1.8 m^2 and follows an ornamental pattern with engraved shafts inscribed in a square. The piers slenderness ratio (height over circumscribed diameter) is around 9.6, not much different from the typical ratio of 7 and 9 found in (Roca et al. 2013). The equivalent section for piers and the lateral buttresses are shown in **Erro! A origem da referência não foi encontrada.**. A trench was made at the southwest transept, exposing the foundations (Coronelli et al. 2014). From the survey of this trench, the external walls present continuous foundations. The foundation is made of coursed rubble stone masonry, exceeds out at 0.5 m from the footprint of the buttress and is extended down at approximately 2.5 m from the ground level (**Erro! A origem da referência não foi encontrada.**). There is no information available on the foundations of the piers, the soil properties and the water table.

The nave roof is a classic high pitched Gothic roof of about 54º, with a covering span of 11.1 m. The timber trusses, placed with a spacing of 3.5 m and fixed over timber wall plates, form a rigid timber framing system with hinged joints of timber connections and metallic-edged blades. They are configured of a queen post on the lower level and a king post over the level of the straining beam, along with a series of struts (**Erro! A origem da referência não foi encontrada.**a). The whole system appears structurally independent from the nave vaults and extends over the extrados of the vaults by 0.8 m. The roof of the lateral aisles is single pitched of about 8º, with a covering span of 5.0 m. and a spacing of 2.7 m (centre axis) (**Erro! A origem da referência não foi encontrada.**b). On the side of the buttresses, the tie beams rest on wall plates, along with an adjoining post and curved brace timber elements, fixed on a small cantilever, that counteract the bending and vertical forces. From the inner side, the tie beams and principal rafters are attached separately to the walls of the triforium. The external roof coatings in both the nave and lateral aisles are large size lead sheets, attached on a system of timber roof battens.

Wrought iron ties, of 43 mm in diameter, with a coupling system at mid-span and externally anchored to the clerestory walls, by cross shaped pattress plates, run along the nave span, in the extrados of the vaults. The infill consists of a part of rubble masonry and an exterior coating of concrete. The infill height, corresponds to the 84% and 95% of the vault’s rise in the central nave and lateral aisles respectively (**Erro! A origem da**

referência não foi encontrada.). Lastly, the nave of Canterbury Cathedral has 7 pairs of flying buttresses, attached in between the nave's clerestory walls and the vertical buttresses, with a thickness of 0.7 m (**Erro! A origem da referência não foi encontrada.**).

5 Material properties and inelastic behaviour

The material properties were determined according to literature and the Italian standards (NTC 2018), in which the mechanical characteristics of masonry structures are defined by means of prescribed values and knowledge levels. In the current study, three types of materials are defined: Caen limestone masonry, describing the entire skeleton of the cathedral; irregular and inhomogeneous masonry, used as infill; and wrought iron for the ties and anchor plates.

The walls consist of a three leaf masonry, with two external leaves from Caen stone masonry and an infill of lime mortar and rubble small fragments. The connection is ensured with long through stones, placed transversely (Foyle, Greshoff, and Newton 2013). Technical information of the Cintheaux quarry, reported by Kock et al. (2015), characterize the compressive strength and mass density of Caen limestone, in which the lower values of 25.9 MPa and 2.050 kg/m^3 were adopted, respectively. The mortar joints were assumed to be of pure lime mortar, of the weakest compressive strength f_m, according to the Italian code; M2.5 (f_{mk}=2.5 MPa). Thus, the characteristic compressive strength of Caen masonry, composed by natural squared stone elements and mortar joints of thickness 5-15 mm, validated by the average compressive strength of its components is f_{bk}=6.7 MPa (NTC 2018 TABLE 11.10.VII; Magenes and Penna 2009; Foti, Debernardis, and Paparella 2012). Due to the lack of material testing, the Knowledge

Level considered is LC1, corresponding to a Confidence Factor of 1.35 (NTC 2018). Thus, the reduced compressive strength of Caen stone masonry is the following:

$$f_{bk,red} = \frac{f_{bk}}{FC} = 5.0\ [\mathrm{MPa}]$$

Regarding the tensile strength of Caen stone masonry, a specific relation between the tensile strength and the compressive strength is difficult to establish. Because of the low tensile bond strength in the unit mortar interface, which is typically in the range of 0.1 to 0.2 MPa (Lourenço 2008), the chosen value for the tensile strength of Caen stone masonry is considered equal to 0.2 MPa.

Given the lack of experimental testing on site and the uncertainty of the level of regularity of the Caen stone masonry, values of modulus of elasticity for regular and irregular stonework range between 4500 MPa and 1700 MPa (Lourenço 2008), so a value of 3000 MPa is considered.

Regarding the infill and due to the high heterogeneity, the mechanical characteristics were taken from reference values for irregular type of stone masonry (Table C8.5.I. of Circolare n.7 2019). The level of knowledge is set to LC1 and the minimum of the range values is chosen, as 1.0 MPa for the compressive strength, 690 MPa for the modulus of elasticity and 19 kN/m^2 for the mass density. The tensile bond strength was chosen as 0.1 MPa (Lourenço 2008). Finally, the mechanical properties of wrought iron ties and anchor plates were defined based on (Holický and Marková 2005) and they are presented in Table 1.

The objective of a simulation of masonry is to represent the transition from the elastic to the quasi brittle behaviour that involves cracking, leading eventually to failure. The inelastic behaviour evolves from the state of a diffused pattern of micro-cracks to localized macro-cracks (Lourenço 1998) and is quantified by the fracture energy G_f for tension and G_c for compression, quantities that are considered material properties (Lourenço 1996). Tensile stresses diminish exponentially, while compression combines a hardening and a softening phase (Lourenço 1998). The adopted mechanical properties and the fracture energy values for all materials are presented in Table 1 (Lourenço 2014).

6 Damage and deformation survey

The final configuration of Gothic Cathedrals is often the result of a sequence of construction phases, for which the structural elements might have undergone different equilibrium conditions. In particular, the optimal state of thrust equilibrium can be reached only when the structure is completed. Therefore, the construction sequence can induce initial deformations and even structural damage (Roca et al. 2013).

A possible construction sequence for Gothic cathedrals consists first of the erection of piers, buttresses and lateral aisles, along with their vaults and nave timber roof. The next stage involves the construction of the nave vaults. During this intermediate stage a system of horizontal pole fittings is implanted and wedged on the top and bottom of the vertical elements. This system together with nave's roof trusses provides a temporary support, centering and protection against tilting of the inner piers, counteracting also the inward lateral trust from the vaults. In case of early removal of the centering or the temporary support system, significant large deformations were introduced in the structure (Roca and Clemente 2005).

A damage survey was carried out in the central nave and lateral aisles of the Canterbury Cathedral during May 2014, by the Civil Engineering Department of the University of Minho, Portugal. In the intrados of the vault system, the main documented damage was a distributed crack pattern in the webs, along with moisture stains and discoloration areas. The cracks follow a repetitive pattern throughout the whole nave and lateral aisles, but without resulting to continuing fragmentations. Still, a potential fragmentation of large structural parts is evident. The number and size of the cracks intensifies in sections 2 and 3 (**Erro! A origem da referência não foi encontrada.**).

A series of large cracks is observed, in the transition between the north and south clerestory and side walls and the vaults of the nave and lateral aisles. It can be concluded that the attaching spans are highly confined and undeformable, and eventually the vaults got separated from the side walls, by forming Sabouret's cracks (**Erro! A origem da referência não foi encontrada.**) (Theodossopoulos 2008).

Another set of cracks are observed above the springings of the inner adjacent span in both the north and south aisle and follow a circular arrangement around each capital. This type of cracks can be induced by several phenomena, such as excessive thrusts, overloading or insufficient flying buttresses, triggering the spreading of the supports; inwards at the aisles and outwards for the nave. As can be seen from the cross section in **Erro! A origem da referência não foi encontrada.**a, the vault of the south aisle is depicted deformed, which is important as an interpretation of the past behaviour. An outward tilting of the vertical abutments, of around 1% in the level of the aisle vault, is a direct indication of the presence of phenomena that have reset the structural system in a new state of equilibrium (Theodossopoulos et al. 2002).

The flying buttresses 2 and 3 of the south aisle show significant deflection and many joints close to the intrados of the middle span and the extrados, near the springing with the clerestory walls, have failed under tensile and shear stresses (**Erro! A origem da referência não foi encontrada.**b). Following the global deformation of the structure, they appear to be rotating outwards, a phenomenon likely to have been induced by differential settlements in the south part of the foundation soil. A possible reason is explained by the presence of a large historic drain pipe that runs along the south wall of the cathedral, since it was found to be leaking in other locations and it is probably leaking in here as well. Thus, it increases the risk of washing away the fine particles of the foundation soil and causes the settlements (Roca et al. 2013).

Furthermore, large parts of the stone units of the flying buttresses have evident signs of crust formation with exfoliation (**Erro! A origem da referência não foi encontrada.**b). During this process layers of the outer stone surface were subject to a chemical material transformation, in the presence of pollutant gases SO_2 and NO_x, which by reaction with air moisture produce a black crust, that later exfoliates and produces flaking. The rate of deterioration of limestone blocks differs according to the local environmental conditions and would have certainly been more intense in the coal burning urban economy of the 19th century in UK (Blows, Carey, and Poole 2003).

Biological growth consists mainly of minute biological organisms such as mosses and algae, which cover large surfaces of the upper part of the flying buttresses and of higher plants, but only in small areas.

7 Dynamic identification tests

In May 2014 a dynamic identification campaign was performed by the University of Minho. Ambient vibration tests were carried out in the nave and South Aisle of the cathedral to obtain the natural frequencies and mode shapes in the area of interest. The monitoring points were flying buttresses, interior and exterior claddings in the South aisle and nave, as well as points on the extrados of vaults. The tests were carried out in five setups, with one reference accelerometer and three accelerometers in each setup, except setup 5, in which all the accelerometers were changed of position (**Erro! A origem da referência não foi encontrada.**). The transducers correspond to piezoelectric accelerometers with a frequency range of 0.15 to 1000 Hz, measurement range ± 0.5 g and a sensitivity of 10 V/g. The signals were recorded by an acquisition system of 24-bit resolution, with a frequency sampling rate equal to 200 Hz, a duration equal to 15 min and processed by ARTeMIS software (SVS 2019), in which the Stochastic Subspace Identification Method (SSI), namely the Unweighted Principal Components (UPC) Method was used. Setups 1, 3 and 4 aim to obtain the mode shape configuration along the y-y axis, while setup 2 was used for the vertical components along the z-z axis. Setup 5 used for the mode shapes of the nave's vault system in the y-y and z-z axis. Table 2 presents the natural frequencies and damping coefficients of the first 12 modes, ranging between 1.29 Hz and 4.27 Hz and between 1.87% and 6.99%, respectively. The first three modes have very close frequencies (1.29 Hz to 1.73 Hz) and MAC values between SSI and UPC higher than 0.95. The 4th and 8th modes present similar mode shapes (2nd curvature), in which the main differences are related with the inflection point, while the 9th, 11th and 12th modes are of a 3rd curvature with two inflection points (**Erro! A origem da referência não foi encontrada.**a).

The Averaged Normalized Power Spectral Density (ANPSD) graph of the horizontal accelerometers of the setup 5 presents clear peaks with frequencies equal to 1.25 Hz, 1.42 Hz, 1.71 Hz and 4.00 Hz, with the frequency of 1.42 Hz corresponding to a high energy peak in all three accelerometers, which indicates a planar mode (**Erro! A origem da referência não foi encontrada.**b). As for the frequencies of 1.25 Hz, 1.71 Hz and 4.00 Hz the additional ANPSDs are different, specifying a 3D mode. Thus, from the experimental tests, the 1st planar (transversal) mode of the structure is considered the one of 1.42 Hz.

8 FE model generation

A finite element model was built in Midas FX+ Version 3.3.0 Customized Pre/Postprocessor for DIANA software, according to the generated 3D CAD model. The model includes a typical transversal section of the nave, with the vertical abutments (piers, buttresses), the corresponding vaults of the nave and the lateral aisles, the flying buttresses, the resulting part of the adjoining cloister and the wrought iron tie over the vaults, anchored on wrought iron plates (**Erro! A origem da referência não foi encontrada.**).

The base connection of the vertical elements was modelled as clamped, as usual for connections to foundations (note that cracking is allowed). As far as the interaction with the adjacent bays, translations on the y-y (longitudinal) axis of the vaults, arches and wall sections were restrained.

The discretized structural elements were composed of homogeneous masonry materials. The created FE mesh, as shown in **Erro! A origem da referência não foi encontrada.**, is composed by 448061 four-node and three-side isoparametric tetrahedron element; two-node truss elements (for the ties); and 94366 nodes in total (DIANA FEA BV 2019). The cracking and crushing behaviour of the material are described with a nonlinear relationship, through a Total Strain Rotating crack model. A default value of the crack band width is assigned, equal to $\sqrt[3]{V}$, with V the volume of the solid element (DIANA 2019).

The FE model was updated, by correlating the 1st mode shape of the experimental tests (1.42 Hz) and the analytical model, with the modulus of elasticity as the updating parameter. For the other mode shapes, a full model of the cathedral would be required. The updated value of modulus of elasticity is 3535 MPa and the obtained mode shapes are shown in **Erro! A origem da referência não foi encontrada.**. The 1st, 3rd and 5th modes are in phase, whereas the 2nd, 4th and 6th modes are configured in a symmetric (out of phase) pattern. The 7th to 12th modes are local modes of in plane and out of plane movement of pinnacles. The 13th and 14th modes are first order local modes of the columns, whereas the 15th and 16th are second order local modes of the columns, involving also partly the pinnacles and side naves. As shown in Table 3, the 1st mode has the highest modal participation mass towards the horizontal direction (67%), whereas for the vertical direction, mode 6 has the highest modal participation mass (40%).

9 Understanding existing damage

Various static nonlinear analyses were carried out, taking into account different hypotheses, in order to differentiate the existing damage and to investigate the level of safety of the cathedral's nave, subjected to self-weight, lateral forces and foundation settlements. Uncertainty was also considered, regarding the infill volume at the aisles and nave's vault pockets, the lateral thrust component from the nave roof, construction process and lastly soil settlements of the south part of the typical section (as a water drainage is present and some signs of possible settlement are visible).

9.1 Self-weight

The built FE model depicts the current state of the typical bay, with the current infill height. A truss with hinge joints and no lateral thrust was considered for the structure of the nave roof. Thus, an equivalent vertical distributed load was applied on the top of the clerestory walls of the model (12.7 kN/m^2).

As seen in Figure 16, the bay appears to deform in a symmetric way, with the upper part of the piers and the clerestory walls spreading and bending outwards, counteracting the thrust from the main vault, which does not appear to be taken by the system of flying buttresses. At the springing of the aisle vaults, the lateral thrust pushes the piers inwards, whereas the vertical buttresses deform by rotating outwards, as observed in many Gothic cathedrals. The cloister appears to restrain and stiffen the lower level of the north buttress. The maximum horizontal displacement (0.86 cm) is located at the outer north pinnacle and the maximum vertical displacement (1.0 cm) is at the nave crown. Due to the inward deformation of the clerestory walls, the tie is under compression which is not expected for this type of element. In order to better understand this behaviour, a self-weight analysis was also performed without the tie. A comparison for the opening of the span at the level of the tie shows: a) with the tie beam, it reduces 1.17mm; b) without the tie beam, it reduces 1.33mm. A difference of 0.16mm indicates that the presence of the tie has a low contribution for the response of the numerical model.

From the load displacement diagrams, depicting the spreading at the cross section of the nave and lateral aisles vaults, it is evident that at around 40% of self-weight there is a significant loss of stiffness, which amounts to 26% for the nave vault and 52% for the lateral vaults. The above loss of stiffness corresponds to damage in the lateral vaults, with cracking at the intrados, surrounding the columns and located at the level of the infill, which agrees well with the documented cracks. In the extrados of the vault, close to the level of infill there is also cracking, while at the transition between the vaults and the aisle windows, cracks are formed, which match the existing Sabouret's cracks (Figure 16 and **Erro! A origem da referência não foi encontrada.**).

The north and south flying buttresses crack at the extrados, close to the outer pinnacles, when the dead load reaches 80%, while the nave vault remains with no cracks. It is also noted that the crack width is quite small, reaching values about 0.5 to 1 mm in the inner part of the south and north aisle vaults.

In order to account for the possibility of horizontal thrust from the nave roof trusses in case of roof excessive deformation, adjustments in the timber joints or other effects, two nonlinear static analyses were performed, with a lateral distributed load applied on top of the south clerestory wall, equal to 1/3 and 1/2 of the vertical component.

The difference found in terms of load-displacement diagrams is marginal, which is justified by the fact that the weight of the roof is relatively small compared to the heavy stonework and does not affect the structural behaviour of the cathedral's bay.

Next, three different infill depths were considered as possible past depths that were altered with respect to the current one (5.8 m in the nave and 3.8 m in the lateral aisles). Through the correlation with the damage maps, the concrete layer was estimated at around 0.40 m depth and placed above the past infill level. A third infill depth, corresponds to a rule of practice for the design of Gothic cathedrals, equal to the 1⁄3 of the free rise of the vault and is 2.1 m and 1.8 m for the nave and the vaults respectively (Huerta 2004).

In the current state of the cathedral's bay, the maximum vertical displacement of the crown at the nave vault is 9% and 23% larger than the one corresponding to the "past estimated infill" and the "reference height" respectively, which is logical, considering the grater counteracting thrust (**Erro! A origem da referência não foi encontrada.**). For all three types of infill, a significant loss of stiffness is obtained with 40-50% of self-weight, which can be interpreted as tensile failure in the webs of the lateral aisles. From then on, the deformations in nave and aisle vaults engage in a linear estimated function.

The crack pattern is related to the spreading and deformation of the aisle vaults and to the additional level of infill, as shown in **Erro! A origem da referência não foi encontrada.**a-c. The total displacements in all three cases are very low but it is interesting to observe that the reference height of traditional Gothic provides the stiffer (i.e. less cracked) condition. The cracks produced from the inward spreading of the piers, in both lateral vaults, appear close to the longitudinal vertex and their exact position is associated with the level of infill, except in the case of the reference infill height. The tensile damage of the current infill state is magnified, with a wider distribution along the thickness of the vault, compared with the other two cases. This difference is related to the additional stiffness from the infill, which suppresses the vault from deforming and thus it cracks at the less stiff part, close to the longitudinal vertex. Nevertheless, all three models are not able to reproduce the crack pattern in the intrados of the south flying buttress, near the springing line with the clerestory walls, which indicates that the typical bay, besides the dead load, is subject to additional effects that compromise its structural stability.

9.2 Phased analysis

In this section, the influence of the construction process on the structural damage and deformation is investigated with a phased nonlinear analysis. Different structural elements are activated in each phase and initial boundary conditions of the stress and deformation field of the previous phases are considered. Since no specific knowledge on the construction sequence was retrieved for this particular cathedral, an assumed construction sequence, related to the vertical progression of structural elements, was accounted based on Roca and Clemente (2005). This considers the possibility of construction of the vaults without the use of temporary stabilizing devices such as braces or ties. According to this hypothesis, the stability of the structure during the intermediate construction stages would rely on the self-capacity of the vaults to remain stable during a limited period of time. The FE model of the critical section is partly activated: the cloister and the piers until the springing level of the lateral vaults, at the 1st phase; the construction of the lateral vaults with the infill, at the 2nd phase; the inner piers rise until the level of the springing of the nave vault at the 3rd phase; at the 4th phase, the rest of the structural elements are activated, including the external buttresses, the clerestory walls, the flying buttresses and the nave vaults with the infill; at the last phase, the wrought iron ties and anchor plates are incorporated (**Erro! A origem da referência não foi**

encontrada.).

As shown from the load-displacement diagram of the span opening (in the south lateral vault), a large inward thrust, at the very early stage of the activation of the aisles in phase 2 and the triforium in phase 3, results in significant tensile damage in the intrados of both the lateral vaults. This is consistent with the observed damage (**Erro! A origem da referência não foi encontrada.**, **Erro! A origem da referência não foi encontrada.**). The resulting final deformation is more than twice than the one corresponding to a conventional self-weight analysis (static nonlinear analysis). This fact stresses the significant damage and deformation during the construction process, where the final configuration is not yet established. The amount of structural damage at phases 2 and 3 is higher, than in the actual structure, given the lack of supporting provisions, however is indicative of the actual triggering mechanism and deformation initiated at an intermediate structural equilibrium stage. Lastly, at the very last stage, the axial force in the tie is 0.1kN, which stresses the fact that only with the application of prestressing (or with the consideration of long term effects) the tie is effectively activated.

The phased analysis justifies clearly some of the damage detected but is still unable to reproduce all the crack pattern observed, indicating that a complementary origin of damage is likely.

9.3 Soil settlements

In order to incorporate the hypothesis of a non-uniform displacement field in the final configuration of the typical bay, more in agreement with the existing crack pattern, vertical displacements were applied at the base of the south buttress, right after the self-weight. The vertical displacement increases until the numerical damage correlates best with the observed damage: i.e. an initiated crack width of 1 mm in the centre point of the thickness, in the middle span of the south flying buttress.

After the application of the self-weight, the translation of the south buttress imposes tensile strains in the area of the observed crack at the inner part of the south aisle vault, but in an inversed way with the hinge at the intrados (**Erro! A origem da referência não foi encontrada.**). The first tensile cracks at the extrados of the south flying buttress near the left spring line reaches 1 mm width for 2 cm of displacement at the base. For a settlement of 5 cm, such damage propagates and cracks larger than 1 mm appear at the intrados of the middle span. At the same time, 0.5 mm cracks are visible at the extrados, in a better agreement with the observed damage. The nave vault suffers a longitudinal crack at the intrados, near the vertex and the outer part of the south aisle vault experiences a crack at the intrados at 2.5 cm displacement. Due to the high values of lateral thrust of the nave vault, the clerestory walls move outwards but their upper part moves inwards. This makes the iron tie non-functional as it is subject to compressive stresses in all the analyses steps.

From the current analysis, soil settlements imposed in the proximity of the south part of the foundations (**Erro! A origem da referência não foi encontrada.**b) are likely to be the most relevant mechanism for the observed damage.

10 Safety assessment

UK is located far from the boundaries of tectonic plates. As an intraplane area, the levels of seismicity are low (Musson and Sargeant 2007). Nevertheless, explaining the seismic activity of the country has been a topic of interest since 1884. The first contour maps of hazard, based on probabilistic assessment, were developed only in 1996 (Musson and Winter 1996). Regarding the design of structures for earthquake resistance, the UK National Annex to Eurocode 8 (NA to BS EN 1998-1:2004 2008) refers to the recommendations given in (PD 6698 2009), where two seismic hazard maps for return periods (T_{NCR}) of 475 and 2500 years are reported. Canterbury is located in a zone with Peak Ground Acceleration (PGA) ranges of 0.00-0.02g (T_{NCR} = 475) and 0.02-0.04g (T_{NCR} = 2500).

A safety assessment allows to understand the behaviour of the structure in order to predict its future performance. The information provided by this type of evaluation can be generalised and help defining the behaviour and the needs of similar structures under seismic actions, mainly regarding: typical collapse mechanisms, areas of concentration of damage, specific structural requirements, repairing or retrofitting for preservation.

This section presents an analysis of the case study under vertical and lateral actions. In order to monitor the progression of tensile cracking and crushing zones until the global failure of the typical bay and evaluate the present safety of the cathedral, the dead load in the model, with the current level of infill, was increased to obtain the vertical capacity using nonlinear static analysis, both in a conventional approach and considering a phased analysis. The latter allows to evaluate the influence of the constructive process. Both analyses were performed including the imposition of differential settlements. Therefore, 4 load cases are considered: 1) gravity loading increase (NonL-Z); 2) gravity loading plus settlements plus gravity load increase (Settle_NonL-Z); 3) phased analysis of gravity loading, followed by gravity load increase (Phased_NonL-Z); and 4) phased analysis of gravity loading, followed by settlements, followed by gravity load increase (Phased_Settle _NonL-Z). Here, it is noted that the increase of gravity loading does not increase settlements, which seems reasonable if the source of settlements is removed (drainage) or the soil has consolidated.

A comparison of the results is presented in **Erro! A origem da referência não foi encontrada.**: the maximum vertical capacity is not significantly affected (≈3%) by the construction process. Nevertheless, it is evident the increment (≈25%) in the stiffness for the initial segment of the curve under self-weight. The phased analysis confirms that, considering the construction process, the structure gains, initially, stability due to the increasing vertical load before the presence of the vault inducing lateral thrust. In the conventional nonlinear analysis, instead, the thrust of the vault affects the building from the very beginning of the process. However, differences are not significant and phased analysis is more computationally expensive. Without loss of generality, in the following only the results of the conventional nonlinear analysis are discussed.

The maximum applied vertical load was 2.8 times the self-weight (NonL-Z in **Erro! A origem da referência não foi encontrada.**). At that point, areas in the springings of the nave and lateral vaults are close to crushing, as shown in **Erro! A origem da referência não foi encontrada.**a, b. The failure mechanism consists of large outward rotations for the clerestory walls. The piers follow a second order deformation, as they are partially constrained by the system of lateral vaults and counteract with the large thrust from the nave vault. The lateral aisles are pressed inwards. At all points of high curvature, tensile damage zones form, reaching deep in the structural parts. The nave vault, cracks along the vertex and crushing zones are evident at the last stage of analysis, close to failure at the springing of the nave vault and in the spring line of the lateral vaults with the piers (**Erro! A origem da referência não foi encontrada.**a, b).

The safety margin, under the presence of vertical loading and soil settlements in the south buttress, is assessed. The displacement field applied at the base of the south buttress is the chosen reference point of 5 cm displacement. The maximum vertical load is 2.6 times the dead load, decreased by 7% from the vertical capacity without settlements (Settle_NonL-Z in **Erro! A origem da referência não foi encontrada.**). A decrease in stiffness is evident, accounting for imposed tensile damage zones by the displacement field at base. The propagating failure mechanism is the failure of the inner springing of the south lateral vault, which is accompanied with large rotations and results to a brittle failure and possibly collapse of the south part of the section as seen in **Erro! A origem da referência não foi encontrada.**c, d and **Erro! A origem da referência não foi encontrada.**. In conclusion, all studied scenarios provide an acceptable safety margin with respect to the self-weight of the structure.

In a second stage of the assessment, the 4 aforementioned combinations of loads are followed by a further nonlinear analysis under a mass proportional lateral load, to understand the seismic performance (not relevant for Canterbury). The lateral load was applied in the x-x direction, following the outward movement of the south buttress. For the sake of clarity, case 1 to 4 became Pushover+X, Settle_Pushover+X, Phased_Pushover+X, Phased_Settle_Pushover+X, respectively. **Erro! A origem da referência não foi encontrada.** shows no significant differences between the curves by comparing the maximum capacity in terms of force. Generally, the responses are ductile and settlements induce a reduction of the stiffness in the initial part of the curve.

As before, in the following, only the results of the Pushover+X curve are discussed. The structure's capacity under horizontal loads is 0.09g (**Erro! A origem da referência não foi encontrada.**), more than double the higher PGA value reported in the hazard maps (PD 6698 2009). After peak load, the horizontal displacement at the nave crown increases, reaching over 0.1m. For the lateral loading, the failure mechanism consists of large deformations of high curvature for the lateral aisles, clerestory walls and the nave vault, with fully formed plastic hinges in several structural elements, where the tensile failure zones have reached deep in the structural parts, mainly in the extrados of the north flying buttress and the south lateral vault, while large vertical and horizontal cracks divide the south buttress near the base (**Erro! A origem da referência não foi**

encontrada.a, b). Through the assessment of the lateral capacity, accounting for the effect of settlements, the structure has a lower overall stiffness, which results in larger deformations at an early stage. The failure mechanism consists of a fully formed hinge in the middle span of the south flying buttress, a group of progressive horizontal cracks in the intrados of the south buttress and several hinge lines along the longitudinal vertex of all the vaults (**Erro! A origem da referência não foi encontrada.**c, d). In conclusion, all studied scenarios provide a similar and rather low seismic capacity for this structure, indicating the need of studies in case of Gothic cathedrals in seismic regions.

11 Comparison with graphic statics

A graphic statics analysis was performed in the transverse cross section of the nave, in order to investigate graphically the global stability of the nave and the level of stresses at the base of the vertical elements. The nave's cross section is discretized in macroelements and the analysis was conducted under self-weight forces, applied at the centre of mass of each voussoir.

An arch is considered stable if any possible thrust line is contained between its boundaries, defined by a maximum and a minimum thrust line (**Erro! A origem da referência não foi encontrada.**a) (Pela and Roca 2014). During the in situ inspection in the nave of Canterbury Cathedral, no cracks were identified in the arcade arches, the clerestory arches of the nave and the arches in the windows of the aisles that could indicate the formation of hinges. Given the fact that the load in the arches is considered mostly uniform and symmetric, the maximum thrust line will be used next in the graphic statics analysis.

The flying buttresses in sections 2 and 3 of the south aisle (see **Erro! A origem da referência não foi encontrada.**), and according to the damage survey, experience significant joint failure in the intrados of the free span, initiated by the spreading of the abutments. Thus, the corresponding thrust line should be close to the state of minimum thrust, which is tangent to a hinge formed at the extrados (Block 2005). For the purpose of conducting the thrust analysis, the minimum thrust line will be assumed with a hinge at the extrados, between two voussoirs (**Erro! A origem da referência não foi encontrada.**b).

As far as the force trajectories, considered in the case of a Gothic quadripartite lierne cross vault under dead load, they follow the steepest descent towards the supports and depending on the curvature of the shells they can either be targeted directly to the supports, coinciding with the principal ribs configuration or through shortest paths, towards the diagonal ribs or even under a superposition of both. The most appropriate force path is dependent on the loading conditions and the geometry of the Gothic vault (**Erro! A origem da referência não foi encontrada.**c) (Block 2009).

The slicing technique, discussed by Karl Mohrmann (Ungewitter 1890) and applied schematically by Wittmann (1879) and Planat (1887), suggests that any three-dimensional vault can be analysed using the 2D thrust line analysis technique, by decomposing the vault into two-dimensional strips. Thus, the web of the vaults is analysed as several 2D arches, which transfer the forces to the diagonal ribs in the form of increments. The ribs later transferred those forces, as diagonal thrusts, to the abutments (Block 2009). In order to obtain the resultant thrust at each quarter of the Gothic cross vaults, with the corresponding infill volume, the resultant force is applied at the centre of mass, which graphically corresponds with sufficient approximation to the plane of the diagonal ribs. Due to the symmetry, an identical thrust component will be applied from the adjoining quarter of the next cross vault. Thus, the two opposite thrust components in a plane vertical to the transversal rib are exempted and the resultant thrust of the Gothic cross vault system in each abutment will be in the plane of the transverse rib. Lastly, in the resultant thrust of the vaults the part from the transversal rib is added (**Erro! A origem da referência não foi encontrada.**d).

The additional forces and points of application from the discretized blocks in the longitudinal and transversal direction, are depicted in force vectors, as shown in **Erro! A origem da referência não foi encontrada.**a. The designed thrust line and the values of the horizontal and vertical components at base are depicted in **Erro! A origem da referência não foi encontrada.**b, where regarding the thrust line in the cross section of the vaults, it corresponds to that of the diagonal ribs. It can be concluded that the structural section of the nave under self-weight, is stable, since a possible line of thrust is contained within its boundaries (Pela and Roca 2014). Regarding the current thrust line, the points of tangency in the extrados of the lateral vaults and the flying buttresses, which correspond to potential hinges, can be matched with the identified cracks on site (**Erro! A origem da referência não foi encontrada.**).

The current equilibrium analysis stands as one of numerous alterative solutions, regarding the force trajectories in the structural elements of the nave. Nevertheless, it is accepted as a sufficient complementary approach, superposed with the results of the FE analyses, as shown in Table 4, which provides excellent agreement.

12 Conclusions

In the current study, the structural assessment and vulnerability of Canterbury Cathedral was conducted, accounting for different hypotheses on causes that could trigger structural damage and can be correlated with existing damage patterns, as defined from the historic research and the in situ damage identification. The current work provides also a basis for discussion on the Gothic cathedrals structural behaviour and damage.

From the existing configuration of the typical bay of Canterbury cathedral, it is evident that the structure can sustain the dead loads and is in good condition, except from minor cracks in the vaults and the south buttresses. A repetitive diffused crack pattern in the intrados at the level of infill of the aisle vaults, surrounding the capitals and the cracks forming in the transition line between the vaults and the side walls, known as Sabouret's cracks, are caused due to self-weight, at an early stage of application. The corresponding cracks are located over tension zones created from the inward pressure of the lateral vaults and the outward bending of the clerestory walls, which counteract the lateral thrusts and result in deflections and 2nd order curvatures in the piers, a common phenomenon found in Gothic cathedrals. According to the results of the phased analysis, the structural damage in the aisle vaults may be induced at an early construction stage. From the deformed configuration it can also be concluded that the flying buttresses, due to their position, do not counteract the thrust from the nave vault. Instead, they force the clerestory walls to bend outwards and they are more likely to work under lateral loads from the roof system itself, which are proven to be not much relevant. The infill volume over the columns appears to correlate with the intensity of the damage and the propagation of tensile failure zones in the body of structural elements, being recommended to adopt the traditional Gothic practice (filling 1/3 of the rise).

The nonlinear static analysis under dead loading and stiff foundations cannot reproduce the existing damage pattern, in particular the cracks and spreading of the south flying buttress in the central sections of the nave. The presence of soil settlements at the south part of the typical bay, at some point during the lifetime of the structure, provides better correlation with the existing crack pattern in the south flying buttress. It seems therefore that foundation settlements were an important triggering mechanism of the documented damage. The different analyses do not significantly alter the maximum capacity of the structure in terms of ultimate vertical loading capacity.

Regarding the vulnerability assessment under vertical and lateral direction, it appears that the structure performs well under vertical loads, as the self-weight can be increased about 2.8 times. The typical bay's capacity under mass proportional lateral load, replicating a seismic scenario, of 0.09g is low (indicate of low seismicity areas) and indicates that the structure cannot withstand large lateral actions, which accounts for the fact that Gothic structural members, such as thin aisle vaults and flying buttresses, have limited capacity to withstand lateral actions, because of tensile damage, under inversion of curvature (Roca 2001). Therefore, studies are highly recommended in case of Gothic cathedrals located in seismic areas. Still, given the local hazard, this capacity can be considered adequate, both for vertical and horizontal loading under current conditions. It is also recommended to perform a parametric analysis, taking into account the uncertainties on the material and geometric properties, aiming at evaluating their influence on response of the structure and improve the knowledge on the structural performance of Gothic cathedrals.

Acknowledgements

The current study has been partly financed by the Dean and Chapter of Canterbury Cathedral and supported by the Morton Partnership Ltd consulting structural engineering company and, in particular, Claudio Corallo.

References

ACNS (Anglican Communion News Services). 2007. Save Canterbury Cathedral Appeal Reaches 7 Million. https://www.anglicannews.org/news/2007/11/save-canterbury-cathedral-appeal-reaches-7-million.aspx.

Block, P. 2005. Equilibrium Systems: Studies in Masonry Structure. Massachusetts, US: MsC Thesis, Massachusetts Institute of Technology.

Block, P. 2009. Thrust Network Analysis Exploring Three-Dimensional Equilibrium. Massachusetts, US: PhD Thesis, Massachusetts Institute of Technology.

Blows, J.F., P.J. Carey, and A.B. Poole. 2003. Preliminary Investigations into Caen Stone in the UK; Its Use, Weathering and Comparison with Repair Stone. *Building and Environment* 38, no. 9–10: 1143–1149.

Canterbury Cathedral. 2011. The World's Oldest Space Frame. https://www.canterbury-cathedral.org/whats-on/news/2011/09/16/the-worlds-oldest-space-frame/.

Canterbury Cathedral. 2012. Completed Corona Is Finally Revealed. https://www.canterbury-cathedral.org/whats-on/news/2012/08/22/completed-corona-is-finally-revealed/.

Canterbury Cathedral. 2013. Stained Glass. http://www.canterbury-cathedral.org/conservation/stainedglass/.

Canterbury Cathedral. 2014. The Great South Window. https://www.canterbury-cathedral.org/whats-on/news/2014/04/07/the-great-south-window/.

Canterbury Cathedral. 2017. Charting the Journey. Spring 2017. https://www.canterbury-cathedral.org/wp-content/uploads/2018/02/Charting-the-Journey-Winter-16-17-for-Partners-Community.pdf.

Canterbury Cathedral. 2019a. The Canterbury Journey Timeline. https://www.canterbury-cathedral.org/heritage/the-canterbury-journey/physicalworks/the-canterbury-journey-timeline/.

Canterbury Cathedral. 2019b. Viridor Credits Awards Grant to Cathedral. https://www.canterbury-cathedral.org/whats-on/news/2019/03/19/viridor-credits-awards-grant-to-cathedral/.

Carfagnini, C., S. Baraccani, S. Silvestri, and D. Theodossopoulos. 2018. The Effects of In-Plane Shear Displacements at the Springings of Gothic Cross Vaults. *Construction and Building Materials* 186: 219–232. https://doi.org/10.1016/j.conbuildmat.2018.07.055.

Collinson, P., N. Ramsay, and M. Sparks. 1995. *A History of Canterbury Cathedral*. Oxford University Press, Oxford.

Coronelli, D.A.M., C.G. Di Prisco, F. Pisanò, S. Imposimato, S. Ghezzi, and M.

Pesconi. 2014. The Tiburio of the Cathedral of Milan: Structural Analysis of the Construction & 20th Century Foundation Settlements. In *15th International Conference on Structural Faults & Repair*, ed. Forde M.C. London, UK: Politecnico di Milano.

D'Ayala, D., and P. Smars. 2003. Architectural and Structural Modelling for the Conservation of Cathedrals. *Journal of Architectural Conservation* 9, no. 3 (January 1): 51–72. https://doi.org/10.1080/13556207.2003.10785351.

DIANA. 2019. Manuals TNO DIANA. http://tnodiana.com/DIANA-manuals.

DIANA FEA BV. 2019. User's Manual -- Release 10.3. Delft, The Netherlands: DIANA FEA BV.

Dudley, C.J. 2010. *Canterbury Cathedral: Aspects of Its Sacramental Geometry*. United States of America: Xlibris Corporation.

Ferreira, T.M. 2019. Notre Dame Cathedral: Another Case in a Growing List of Heritage Landmarks Destroyed by Fire. *Fire* 2, no. 2 (April 24): 20. https://www.mdpi.com/2571-6255/2/2/20.

Filippoupolitis, M. 2011. The South Oculus at Canterbury Cathedral. Guimarães, Portugal: MSc Thesis, University of Minho. http://hdl.handle.net/1822/18896.

Foti, D., M. Debernardis, and V. Paparella. 2012. Structural Safety Control of Masonry Buildings: Non-Linear Static Seismic Analysis with a Non-Linear Shear Strength Criterion. In *Eleventh International Conference on Computational Structures Technology*, ed. B.H.V. Topping, Vol. 99:1–14. Stirlingshire, Scotland: Civil-Comp Press.

Foyle, J., R. Greshoff, and H. Newton. 2013. Chapter 6: Stone Repair and Conservation after 1945. In *Architecture of Canterbury Cathedral*. London, UK: Scala Publishers.

Gaetani, A., P.B. Lourenço, G. Monti, and G. Milani. 2017. A Parametric Investigation on the Seismic Capacity of Masonry Cross Vaults. *Engineering Structures* 148: 686–703. http://dx.doi.org/10.1016/j.engstruct.2017.07.013.

Gaetani, A., G. Monti, P.B. Lourenço, and G. Marcari. 2016. Design and Analysis of Cross Vaults Along History. *International Journal of Architectural Heritage* 10, no. 7: 841–856.

Heritage Lottery Fund (HLF). 2018. *National Heritage Memorial Fund Lottery Distribution Annual Report and Accounts for the Year Ended 31 March 2018*. UK: National Heritage Memorial Fund https://assets.publishing.service.gov.uk/government/uploads/system/uploads/attachment_data/file/731175/Heritage_Lottery_Fund_ARA_2017-18.pdf.

Heyman, J. 2019. The Fire at Notre-Dame: Roof. *Current Trends in Civil & Structural Engineering* 2, no. 5. https://irispublishers.com/ctcse/fulltext/the-fire-at-notre-dame-roof.ID.000548.php.

Holický, M., and J. Marková. 2005. Presentation: Characteristics of Materials. Czech Republic: Czech Technical University in Prague (in Czech).

Huerta, S. 2004. *Arcos, Bóvedas y Cúpulas. Geometría y Equilibrio En El Cálculo Tradicional de Estructuras de FábricaArcos, Bóvedas y Cúpulas. Geometría y Equilibrio En El Cálculo Tradicional de Estructuras de Fábrica*. Madrid, España: Instituto Juan de Herrera.

De Kock, T., W. De Boever, J. Dewanckele, M.A. Boone, P. Jacobs, and V. Cnudde. 2015. Characterization, Performance and Replacement Stone Compatibility of Building Stone in the 12th Century Tower of Dudzele (Belgium). *Engineering Geology* 184: 43–51.

Lourenço, P.B. 1996. Computational Strategies for Masonry Structures. Netherlands: PhD Thesis, Delft University of Technology. http://www.narcis.nl/publication/RecordID/oai:tudelft.nl:uuid:4f5a2c6c-d5b7-4043-9d06-8c0b7b9f1f6f.

Lourenço, P.B. 1998. Experimental and Numerical Issues in the Modelling of the Mechanical Behaviour of Masonry. In *Structural Analysis of Historical Constructions II. Possibilites of the Numerical and Experimental*, ed. P. Roca, J.L. González, E. Oñate, and P.B. Lourenço, 57–91. Barcelona, Spain: International Center for Numerical Methods in Engineering.

Lourenço, P.B. 2008. Structural Masonry Analysis: Recent Developments and Prospects. In *14th International Brick and Block Masonry Conference*, ed. University of Newcastle. Sydney, Australia. http://hdl.handle.net/1822/17176.

Lourenço, P.B. 2014. Presentation SA2_12: Modelling of Masonry and

Homogenization. Guimarães, Portugal: University of Minho.

Magenes, G., and A. Penna. 2009. Existing Masonry Buildings: General Code Issues and Methods of Analysis and Assessment. *Eurocode 8 Perspectives from the Italian Standpoint Workshop Notes*. Napoli, Italy.

Musson, R., and S. Sargeant. 2007. Eurocode 8 Seismic Hazard Zoning Maps for the UK. *British Geological Survey Technical Report*no. CR/07/125: 70.

Musson, R., and P.W. Winter. 1996. Seismic Hazard Maps for the U.K. *Natural Hazards* 14, no. 2–3: 141–154.

NA to BS EN 1998-1:2004. 2008. *UK National Annex to Eurocode 8: Design of Structures for Earthquake Resistance*. London, UK: BSI British Standards.

NTC. 2018. *Norme Tecniche per Le Costruzioni*. *Italian Technical Norms for Constructions.* Rome, Italy.

PD 6698. 2009. *Recommendations for the Design of Structures for Earthquake Resistance to BS EN 1998*. London, UK: BSI British Standards.

Pela, L., and P. Roca. 2014. Presentation SA1_07: Ancient Rules and Classical Approaches Part 1. Barcelona, Spain: Universitat Politècnica de Catalunya.

Planat, P. 1887. *Pratique de La Mécanique Appliquée a La Resistance Des Matériaux*. Paris: Aux Bureaux de La construction moderne.

Ramos, L. 2007. Damage Identification on Masonry Structures Based on Vibration Signatures. Guimarães, Portugal: PhD Thesis, University of Minho. http://hdl.handle.net/1822/7380.

Ramos, L., and P.B. Lourenço. 2014. Presentation SA1_07: Inspection and Diagnosis Applied to Historical Structures. Guimarães, Portugal: University of Minho.

Roca, P. 2001. Studies on the Structure of Gothic Cathedrals. *Historical Constructions*.: 71–90. http://www.civil.uminho.pt/masonry/Publications/Historical constructions/page 71-90 _Roca_.pdf.

Roca, P., M. Cervera, G. Gariup, and L. Pela. 2010. Structural Analysis of Masonry Historical Constructions. Classical and Advanced Approaches. *Archives of Computational Methods in Engineering* 17, no. 3: 299–325.

Roca, P., M. Cervera, L. Pela, R. Clemente, and M. Chiumenti. 2013. Continuum FE

Models for the Analysis of Mallorca Cathedral. *Engineering Structures* 46: 653–670. http://dx.doi.org/10.1016/j.engstruct.2012.08.005.

Roca, P., and R. Clemente. 2005. Studies on the Origin of Deformation and Damage in Long-Span Historical Structures. In *11th International Conference on Fracture*. Torino, Italy.

Roca, P., G. Martínez, F. Casarin, C. Modena, P.P. Rossi, I. Rodríguez, and A. Garay. 2008. Chapter 6: Monitoring of Long-Term Damage in Long-Span Masonry Constructions. In *Learning from Failure: Long-Term Behaviour of Heavy Masonry Structures*, ed. L. Binda, 11:125–152. Southampton, UK: WIT.

SVS. 2019. ARTeMIS Modal, Release 6.0.2.0. Aalborg, Denmark: Structural Vibration Solutions.

Theodossopoulos, D. 2006. Technology and Geometry in the Design of “Gothic” Vaults in Britain. In *Second International Congress on Construction History*, 3:3079–3095.

Theodossopoulos, D. 2008. Structural Design of High Gothic Vaulting Systems in England. *International Journal of Architectural Heritage* 2, no. 1: 1–24.

Theodossopoulos, D., and B. Sinha. 2008. Structural Safety and Failure Modes in Gothic Vaulting Systems. In *International Seminar on Structural Masonry*. Istanbul, Turkey.

Theodossopoulos, D., B. Sinha, A.S. Usmani, and A.J. Macdonald. 2002. Assessment of the Structural Response of Masonry Cross Vaults. *Strain* 38, no. 3: 119–127.

Ungewitter, G. 1890. *Lehrbuch Der Gotischen Konstruktionen: III Auflage Neu Bearbeitet von K. Mohrmann*. Ed. Weigel Nachfolger. 3rd ed. Leipzig, Germany.

Willis, R. 1845. *The Architectural History of Canterbury Cathedral*. London, UK: Longman.

Wittmann, W. 1879. Zur Theorie Der Gewölbe. *Zeitschrift Für Bauwesen* 29: 61–74.

Wright, L. 2011. Canterbury Cathedral Plan-Ceiling Plan | Architecture Portfolio. *June 7, 2011*. https://liamwright.wordpress.com/2011/06/07/124/canterbury-cathedral-plan-ceiling-plan-1-to-200-at-a0-add-on-flattened-final-save-2-for-web/.

Table 1. Mechanical properties of Caen stone masonry, infill masonry, wrought iron ties and anchor plates.

Mechanical properties		Caen stone masonry	Infill loose stone masonry	Wrought iron
Compression strength	fc (MPa)	5.00	1.0	207
Modulus of elasticity	E (MPa)	3000	690	100000
Poisson's ratio	v (-)	0.2	0.2	0.2
Tensile strength	ft (MPa)	0.2	0.1	207
Fracture energy Mode I (tension)	Gf (N/mm)	0.012	0.012	-
Fracture energy Mode I (compression)	Gfc (N/mm)	8	1.6	-
Specific weight	ρ (kN/m3)	21	19	76

Table 2 Frequencies and damping ratios of the first 12 modes.

MODE	FREQUENCY [Hz]	STD. FREQUENCY [Hz]	DAMPING RATIO [%]	STD. DAMPING RATIO [%]
1	1.29	0.13	2.04	0.90
2	1.43	0.01	2.47	1.04
3	1.73	0.02	2.14	0.28
4	2.27	0.14	3.42	1.51
5	2.43	0.01	2.56	1.33
6	2.68	0.04	3.81	2.75
7	2.70	0.01	3.62	2.91
8	3.11	0.04	2.18	0.52
9	3.38	0.02	6.99	7.06
10	3.58	0.03	5.42	4.88
11	4.00	0.04	2.02	1.00
12	4.27	0.03	1.87	1.39

Table 3. Modal participation mass for the first 20 modes at each direction.

MODE	FREQUENCY [Hz]	MODAL PARTICIPATION MASS x-x [%]	MODAL PARTICIPATION MASS y-y [%]	MODAL PARTICIPATION MASS z-z [%]
1	1.42	67.05	0.00	0.00
2	3.30	0.04	0.00	0.96
3	5.29	4.58	0.00	0.05
4	6.43	0.04	0.00	4.24
5	7.20	0.36	0.00	0.00
6	7.81	0.00	0.00	39.64
7	8.38	0.09	0.00	0.05
8	8.84	0.06	0.00	0.55
9	9.19	0.02	0.25	0.00
10	9.29	1.76	0.00	0.11
11	9.30	0.02	0.24	0.00
12	9.40	0.18	0.00	0.64
13	11.16	0.00	3.50	0.00
14	11.17	0.00	2.44	0.00
15	11.40	10.55	0.00	0.03
16	12.19	1.50	0.00	1.05
17	13.61	0.00	9.80	0.00
18	14.42	0.03	0.00	0.00
19	14.50	0.06	0.00	11.23
20	14.75	0.46	0.00	0.59
TOTAL CUM.PERCENT.		86.79	16.23	59.14

Table 4. Comparison between resultant force vectors from the Graphic Statics and Linear Static analysis, in various sections.

Force vectors (kN)	Graphic Statics	Linear Static	Difference
Cloister (base)	633	700	10%
North Buttress (base)	2994	3343	10%
North Pier (base)	2385	2419	1%
South Pier (base)	2385	2437	2%
South Buttress (base)	3402	3596	5%
Left Springing South Flying Buttress	45	39	13%
Right Springing South Flying Buttress	144	130	10%

(a) (b)

Figure 1. (a) Aerial view of Canterbury Cathedral from southeast (photo by John Fielding 2013). (b) The west front aspect of the cathedral in 1821 before the completion of the north-west tower (Collinson, Ramsay, and Sparks 1995).

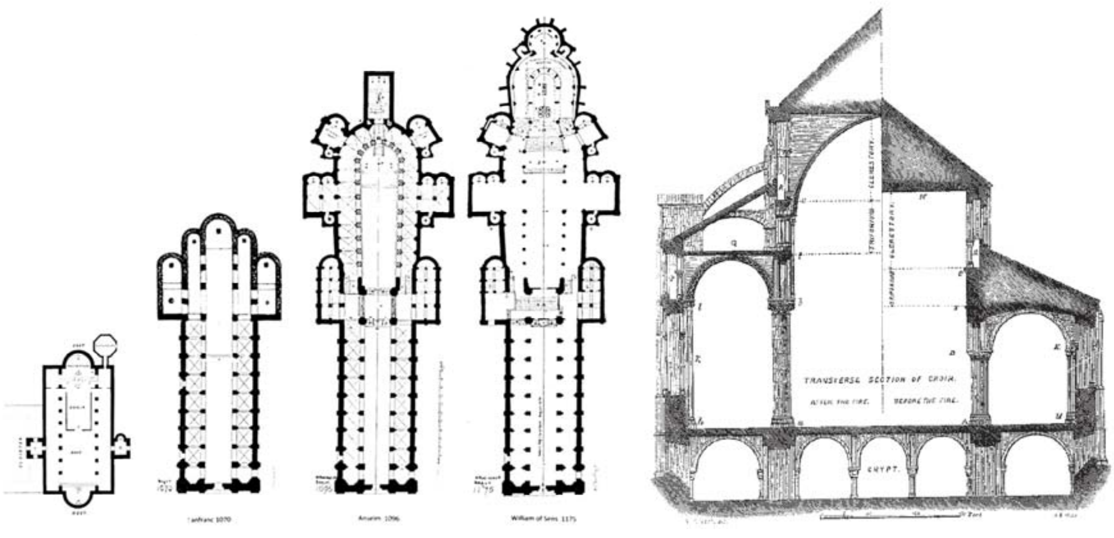

(a) (b) (c) (d) (e)

Figure 2. Ground plans and sections of the cathedral as it evolved over time, from 1025 to 1175. (a) The Anglo-Saxon Cathedral, as believed during the phase IV, (b) the Cathedral of Lanfranc, (c) the Cathedral of Anselm, (d) the Cathedral of William of Sens, (e) transverse section of the choir, with the left part the new Gothic Choir of William of Sens and on the right part the Archbishop Anselm’s Choir (Dudley 2010; Collinson, Ramsay, and Sparks 1995).

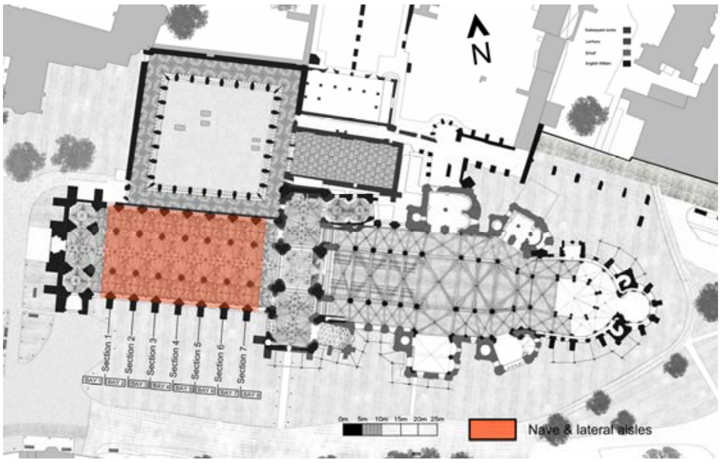

(a)

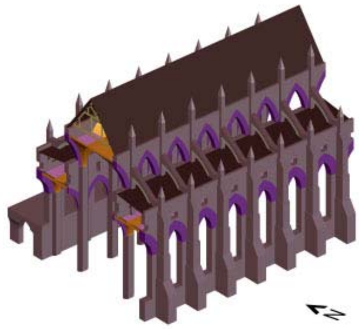

(b)

(c)

(d)

Figure 3. (a) Top plan of Canterbury Cathedral in present time, depicting the nave and lateral aisles area (Wright 2011), (b) geometrical model of the nave, lateral aisles and the adjoining part of the cloister, (c) view of the south aisle, presenting the system of vertical and flying buttresses, (d) view of the cloister arcade, attached to the north aisle.

(a) (b) (c)

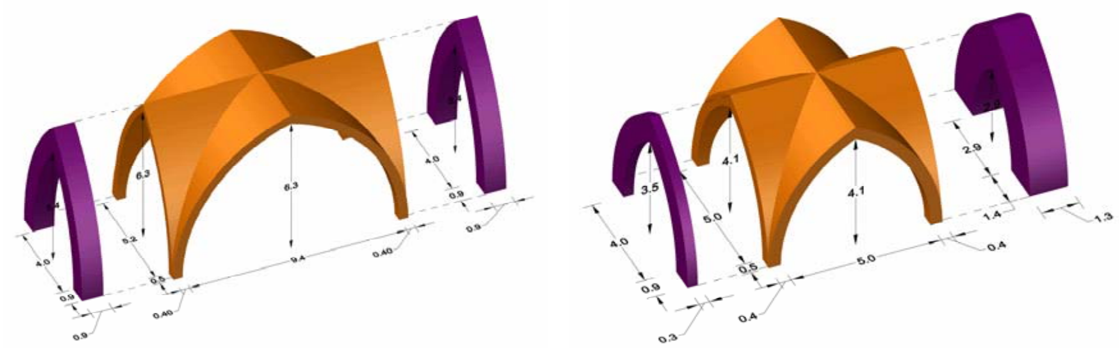

(d) (e)

Figure 4. (a) View of the nave of the cathedral looking east, (b) view of the north aisle of Canterbury Cathedral looking east, (c) view of the south aisle looking east, (d) simplified 3D view of the Gothic cross vault at the nave with the adjacent clerestory arches, including dimensions (meters), as generated for the CAD model, (e) simplified 3D view of the Gothic cross vault at the south aisle, with the adjacent arcade arch (left) and the aisle window arch (right), including dimensions (meters).

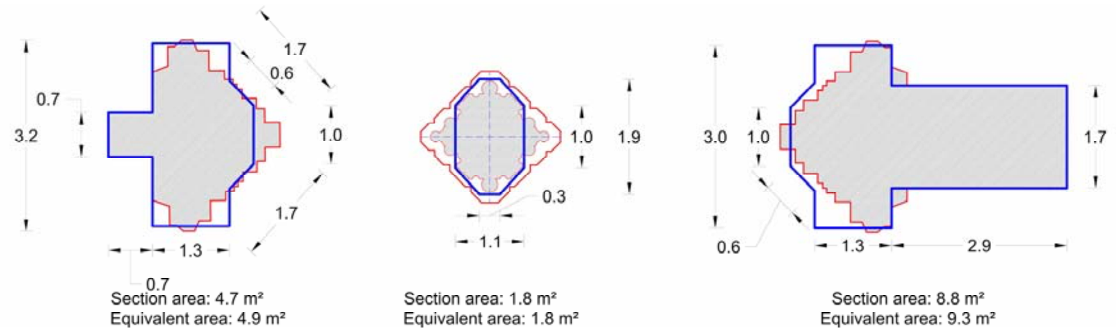

(a) (b) (c)

Figure 5. Sections depicting the actual (red) and chosen (blue) equivalent dimensions (meters) and area of the piers and buttresses, for (a) the north buttress, (b) the pier and (c) the south buttress.

Figure 6. Part of the exposed foundation at the west corner of the southwest transept.

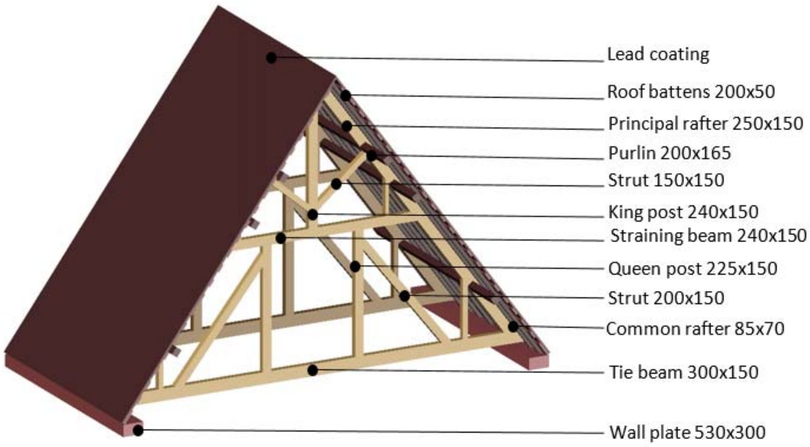

(a)

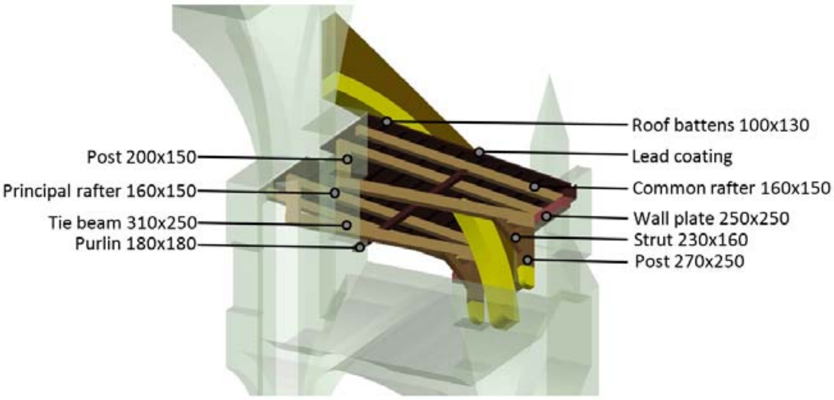

(b)

Figure 7. The roof system of the cathedral: (a) Structural parts of the roof framing in the nave and section areas (millimetres); (b) structural parts of the roof framing in the south aisle of the cathedral and section areas (millimetres).

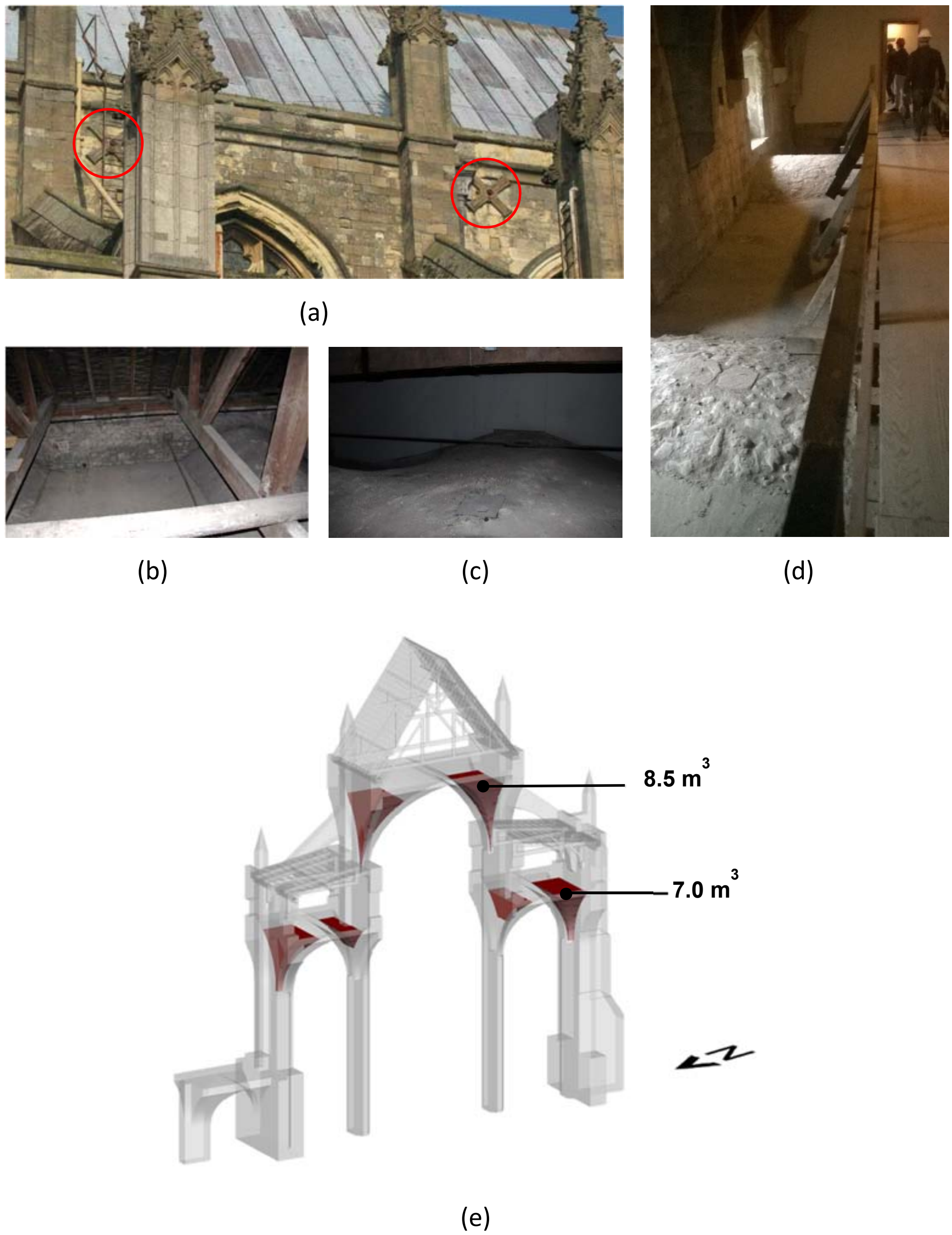

Figure 8. (a) External view of the nave clerestory walls of the cathedral, depicting the two anchor cross shaped plates on the right side of each transverse section; (b, c) infill, cross vault system and roof frame at south aisle roof void; (d) inside views of the roof void in the nave, depicting the iron tie in the clerestory walls above the vaults, with the coupling system at mid-span; (e) infill volumes in 3D representation of the south half nave section of the cathedral.

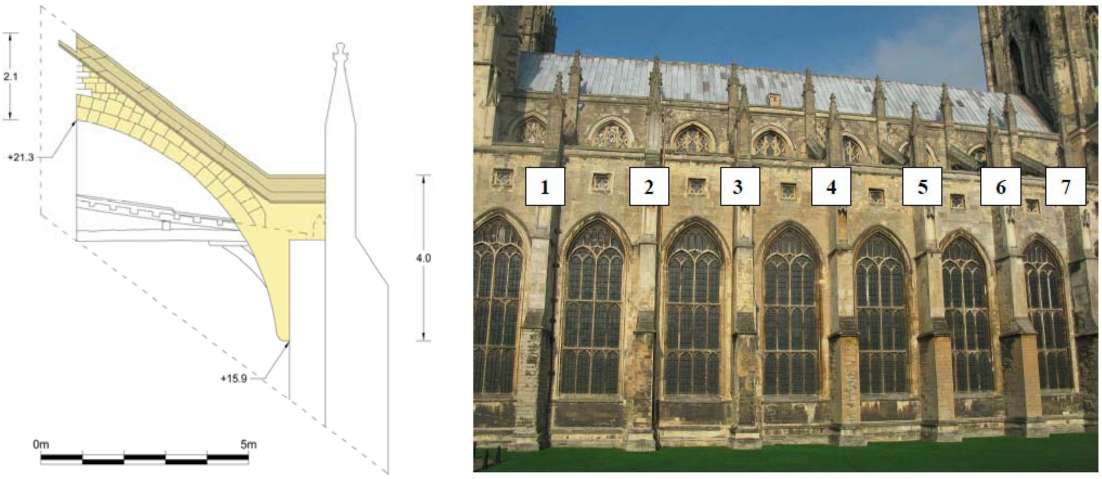

(a) (b)

Figure 9. (a) East view of flying buttress 2 in the south aisle of the cathedral, depicting the connection between the clerestory wall and vertical buttress, as well as elevation levels from the base; (b) view of the South aisle of the cathedral, presenting the numbering of the seven transverse sections.

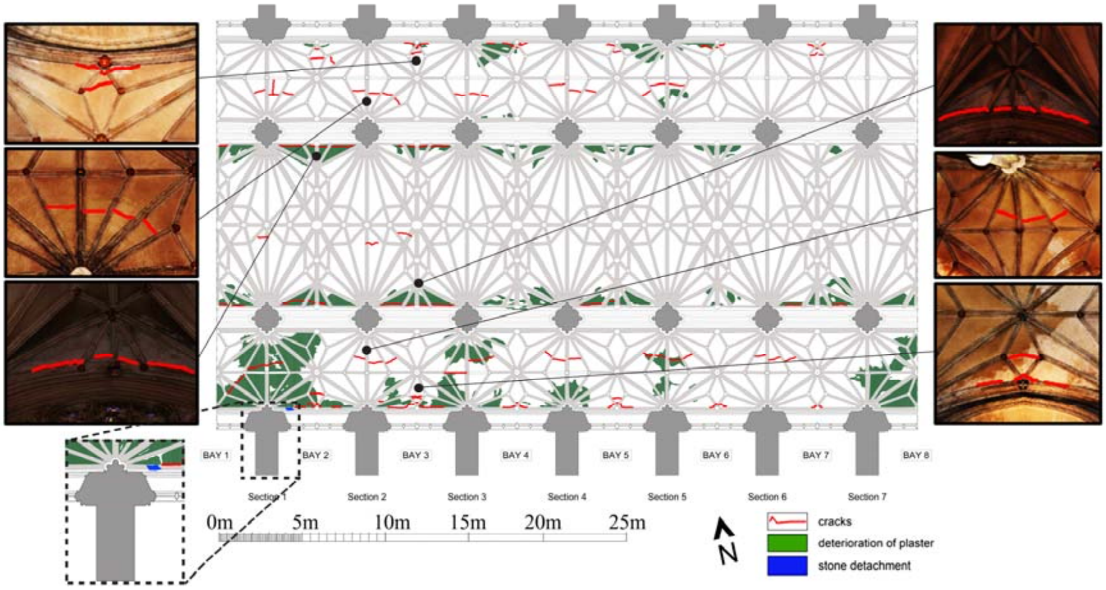

Figure 10. Damage map of the intrados of the vault system in the nave and lateral aisles of the cathedral.

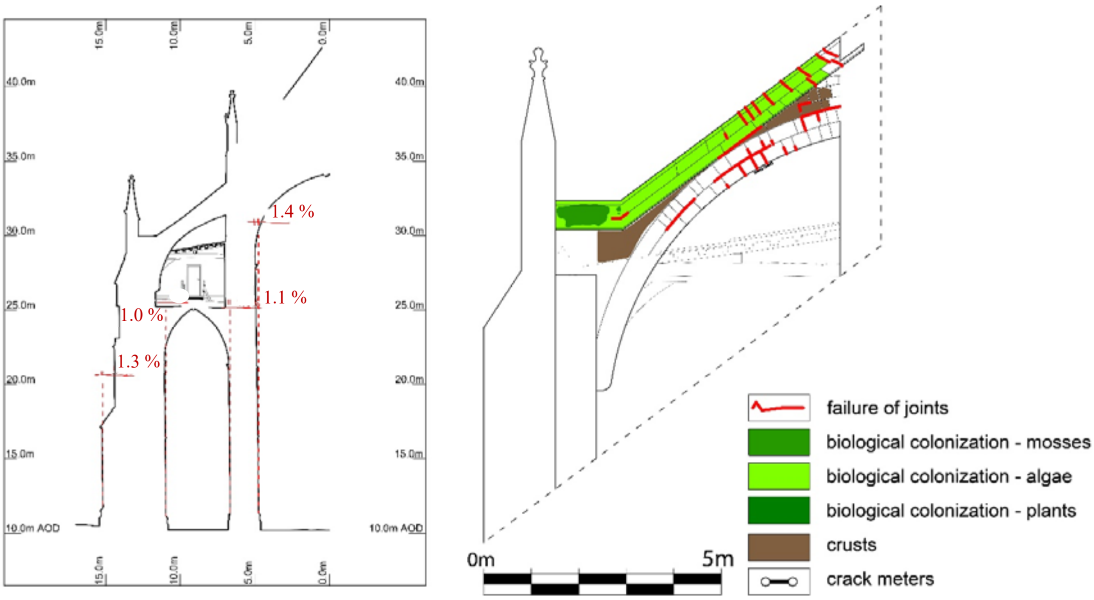

(a) (b)

Figure 11. (a) 3rd from the east cross section, depicting the south aisle and half of the nave, including horizontal deformations with respect to the height, (b) damage map from the west view of the 3rd from the east flying buttress.

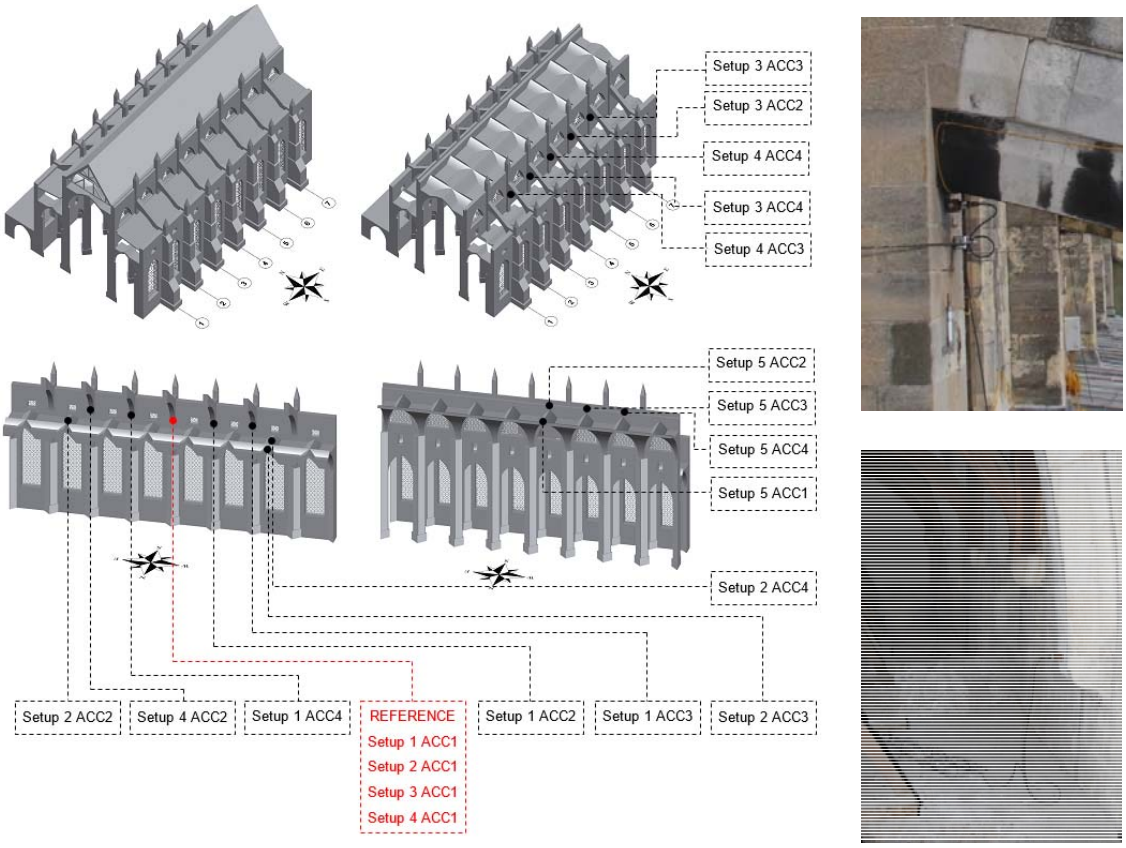

(a) (b)

Figure 12. (a) Disposition of accelerometers in performed setups of the dynamic identification tests (Reference sensors depict in red colour); (b) Measuring equipment: (top) accelerometer on the intrados springing of the flying buttress, (bottom): accelerometer on the exterior cladding of the nave wall.

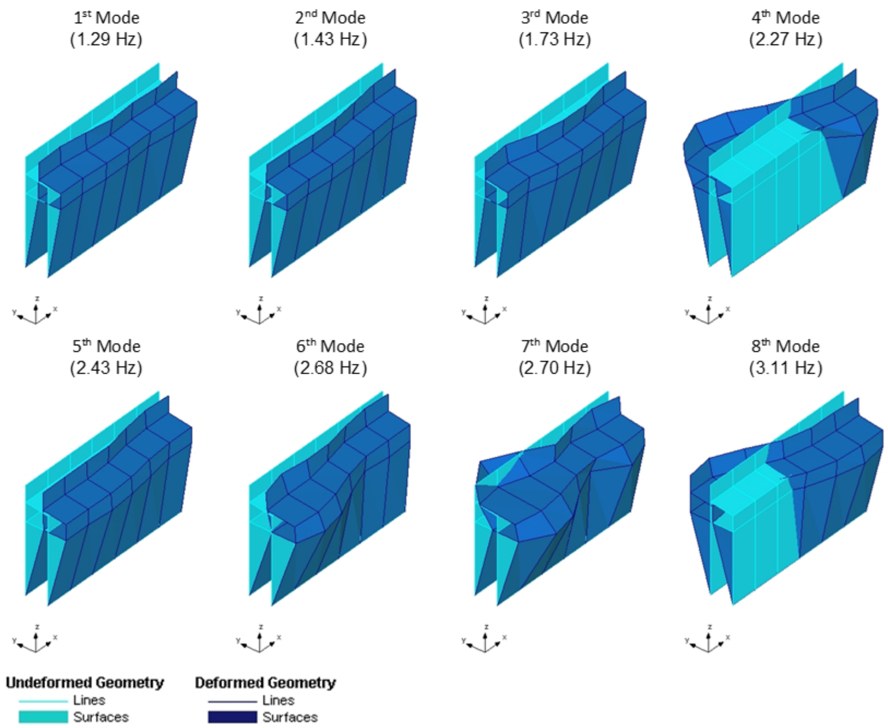

(a)

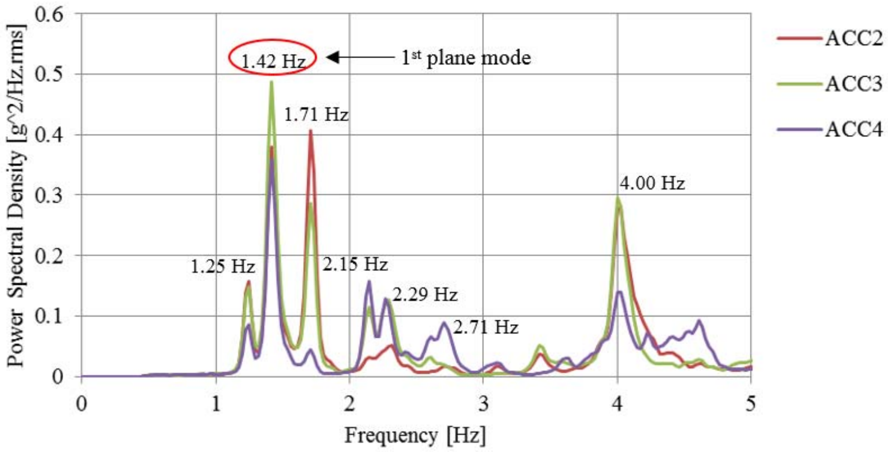

(b)

Figure 13. Dynamic identification tests in the South Aisle: (a) first eight mode shapes obtained from the Setups 1, 3 and 4; (b) averaged Normalized Power Spectral Density for the horizontal accelerometers of setup 5.

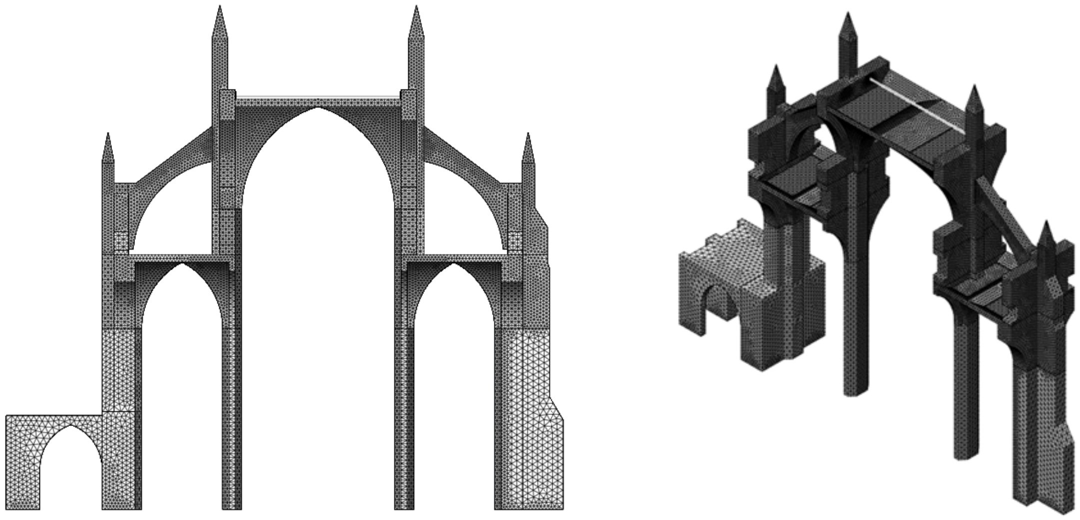

(a) (b)

Figure 14. North – south section looking east (a) and 3D view (b) of the FE model of the typical bay in the nave of the cathedral, showing the mesh.

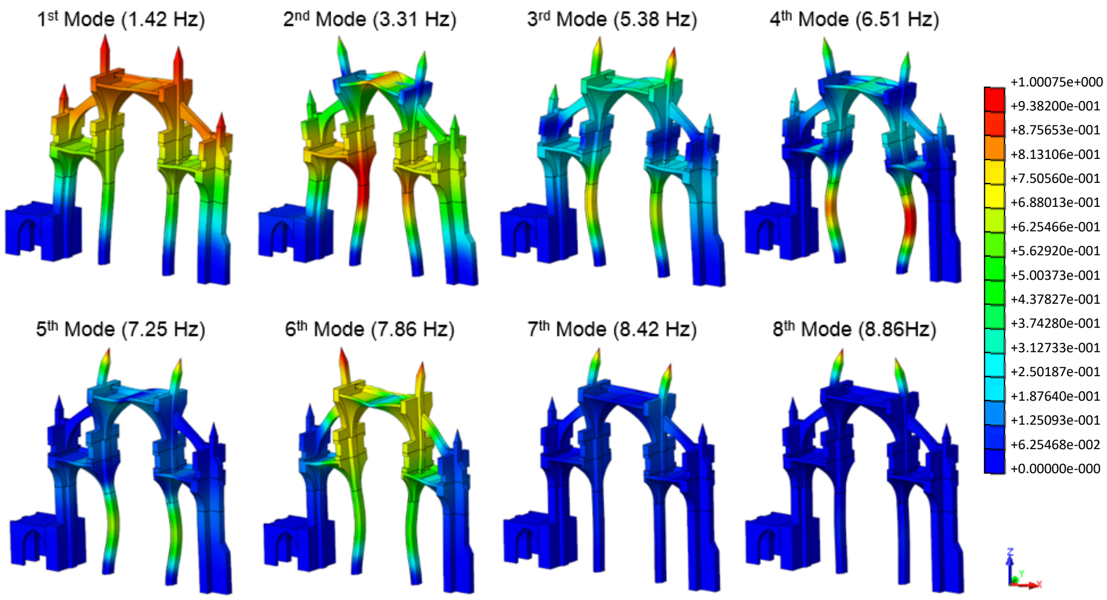

Figure 15. Mode shape configuration of modes 1 to 8, with the natural frequencies.

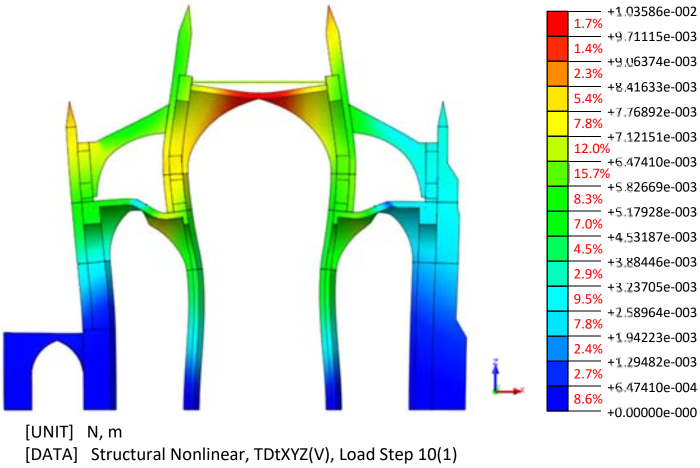

(a)

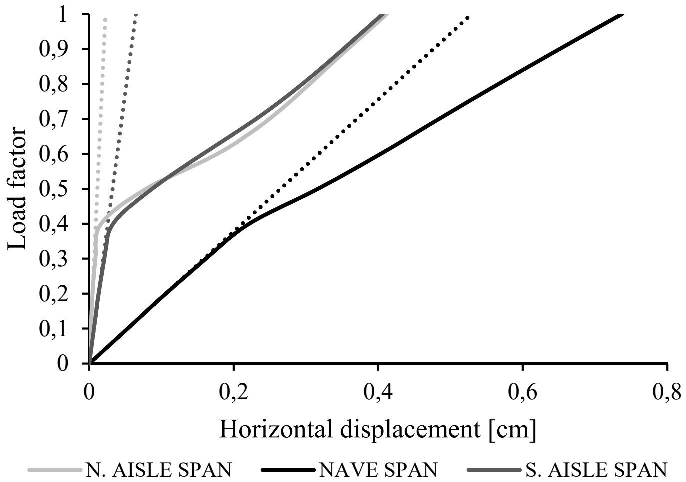

(b)

Figure 16. (a) Deformed shape (x100) at last load step; (b) load displacement diagram of the span opening in the nave and lateral aisles versus the load factor of the self-weight, superposed with the linear response in dashed lines.

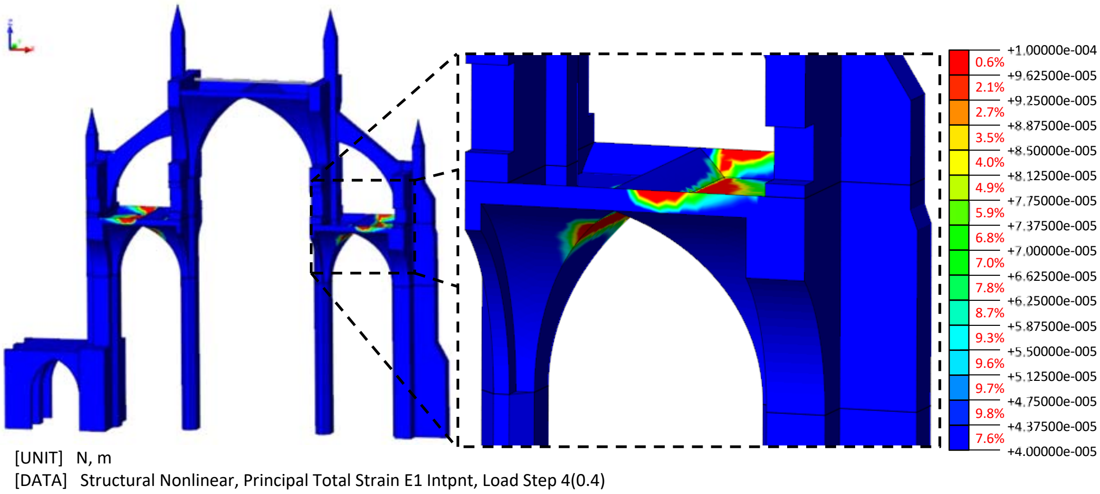

(a)

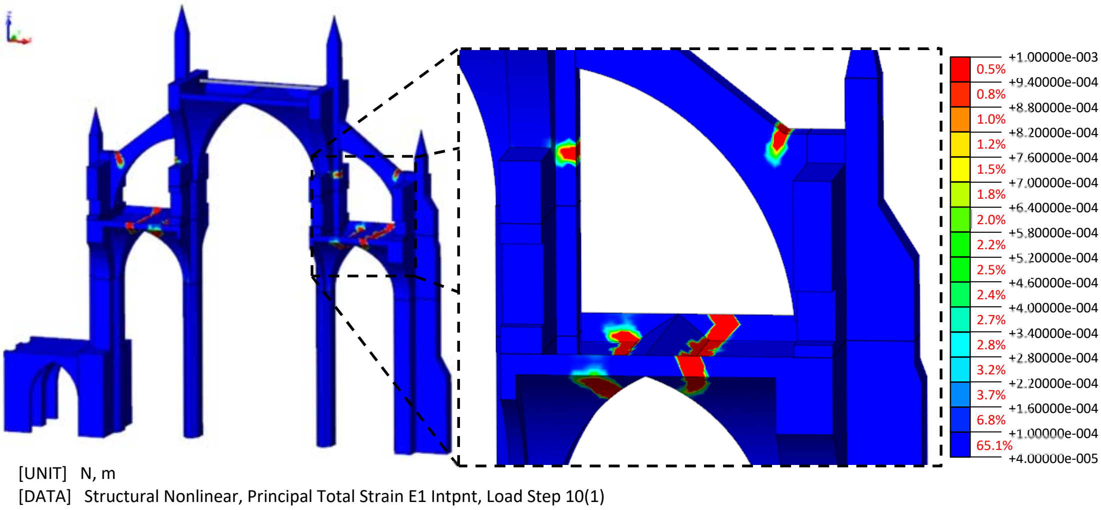

(b)

Figure 17. Nonlinear static analysis under dead-loads: (a) distribution of maximum principal strains at the 40% of dead load; (b) distribution of maximum principal strains at last load step.

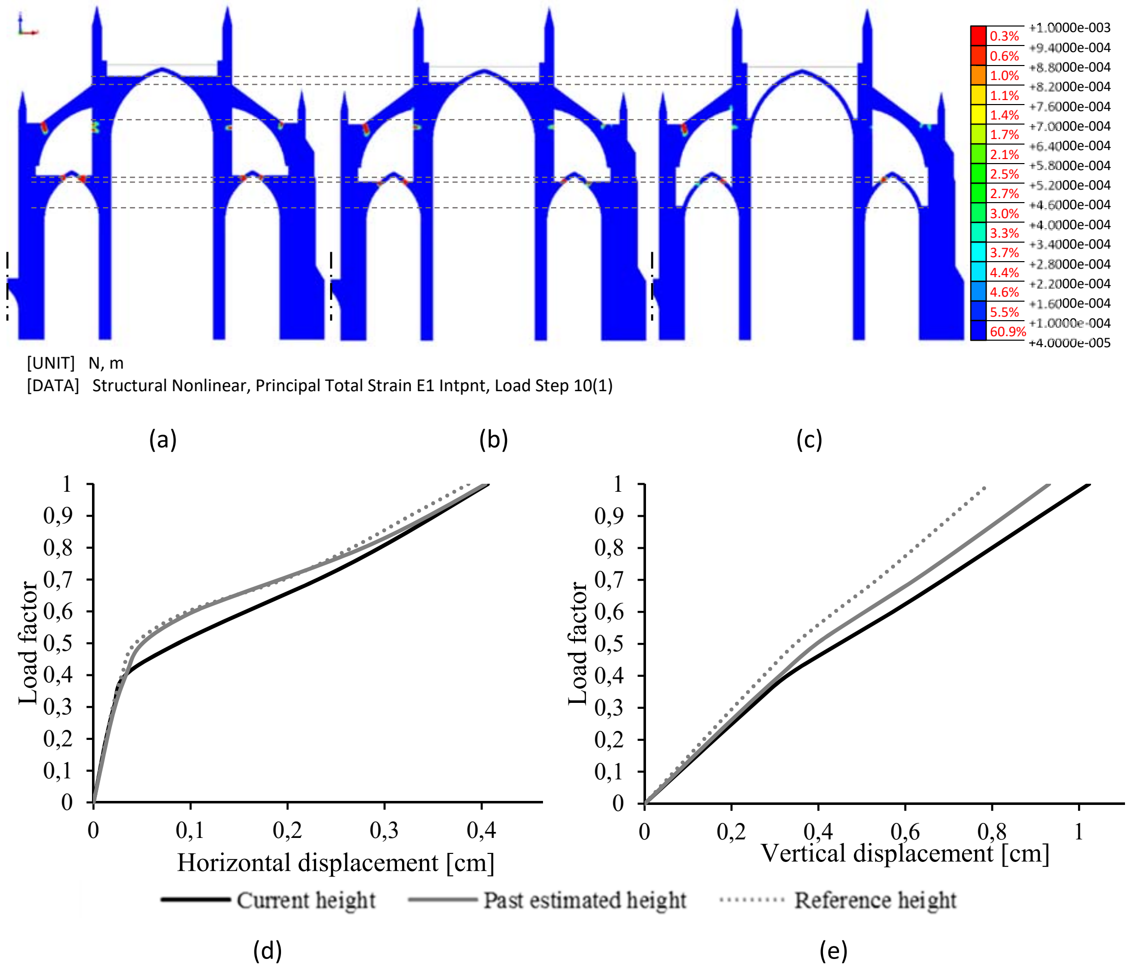

Figure 18. Distribution of maximum principal strains at last load step, in a slicing plane, at the symmetry axis for the current (a), the past estimated (b) and the reference infill height (c), (d) load versus horizontal displacement diagram of the south aisle's crown, (e) load versus vertical displacement diagram of the nave's crown.

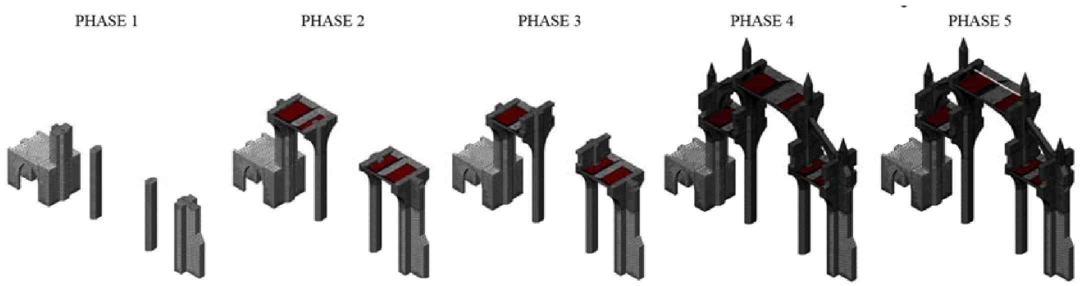

Figure 19. Construction phases of a typical cross section.

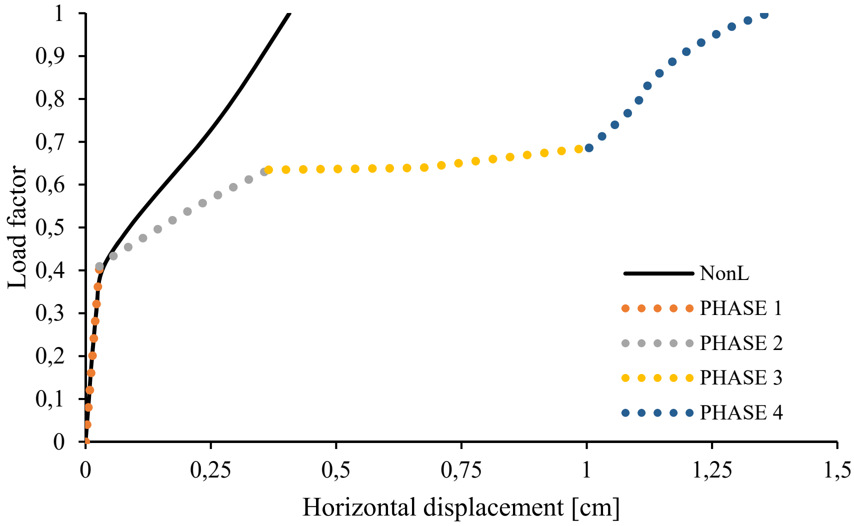

Figure 20. Load factor versus horizontal displacement diagram of the south aisle span opening, for the nonlinear static analysis (NonL) and the phased nonlinear analyses (phase 1 to 4).

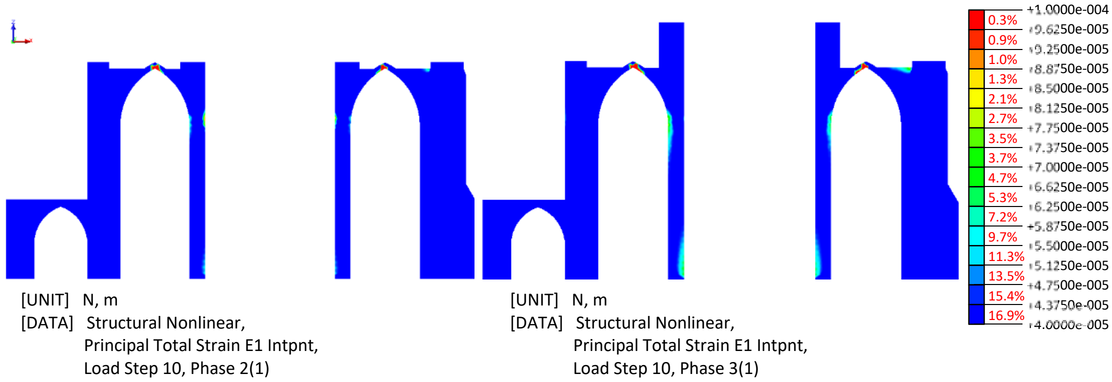

(a) (b)

Figure 21. Distribution of maximum principal strains at last load step of phase 2 (a) and phase 3 (b), in a slicing plane, at the symmetry axis.

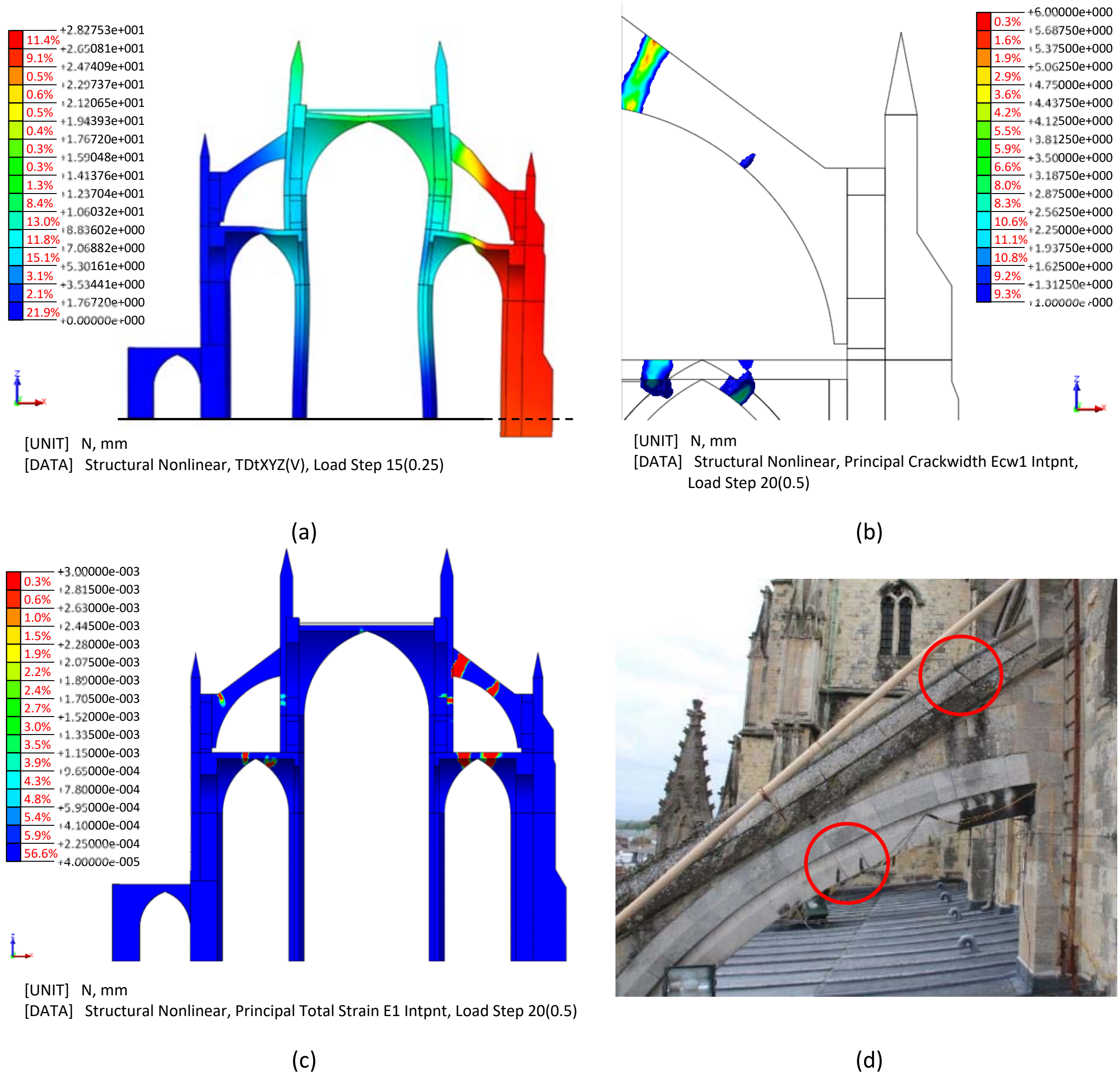

Figure 22. (a) Deformed shape (x100), at a corresponding load step of a 1 mm crack width at the centre point of the middle span of the south flying buttress, (b) crack width distribution at the south flying buttress, with a crack larger than 1 mm, (c) distribution of maximum principal strains, under differential settlements, (d) cracks at the top part and the middle span of the south flying buttress, in section 3.

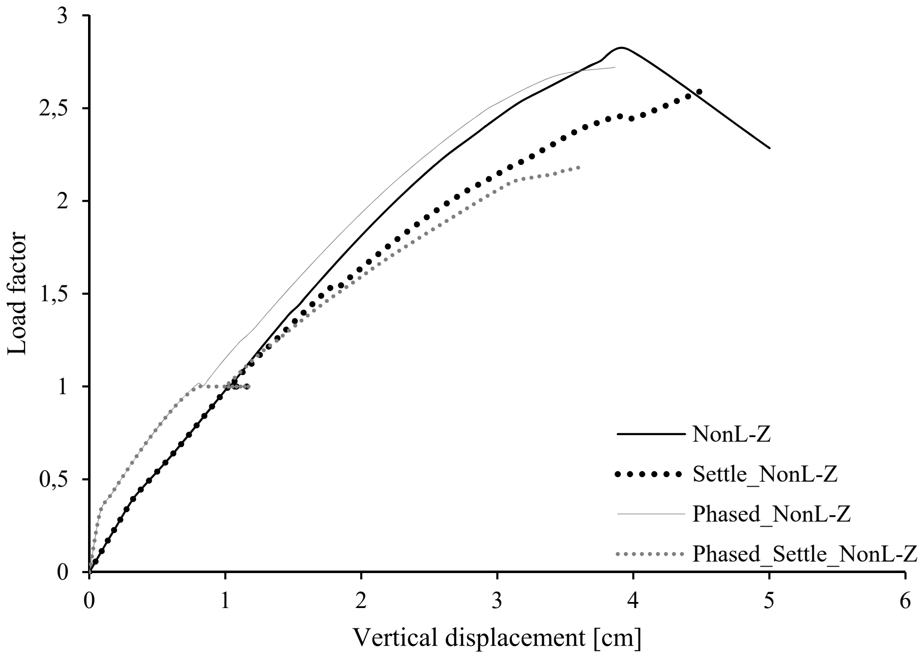

Figure 23. Load displacement diagram, depicting the vertical capacity in terms of vertical displacements of the nave crown: 1) conventional nonlinear analysis in vertical direction (NonL-Z); 2) case 1) with settlements (Settle_NonL-Z); 3) phased analysis followed by nonlinear analysis in vertical direction (Phased_NonL-Z); and 4) case 3) with settlements (Phased_Settle _NonL-Z).

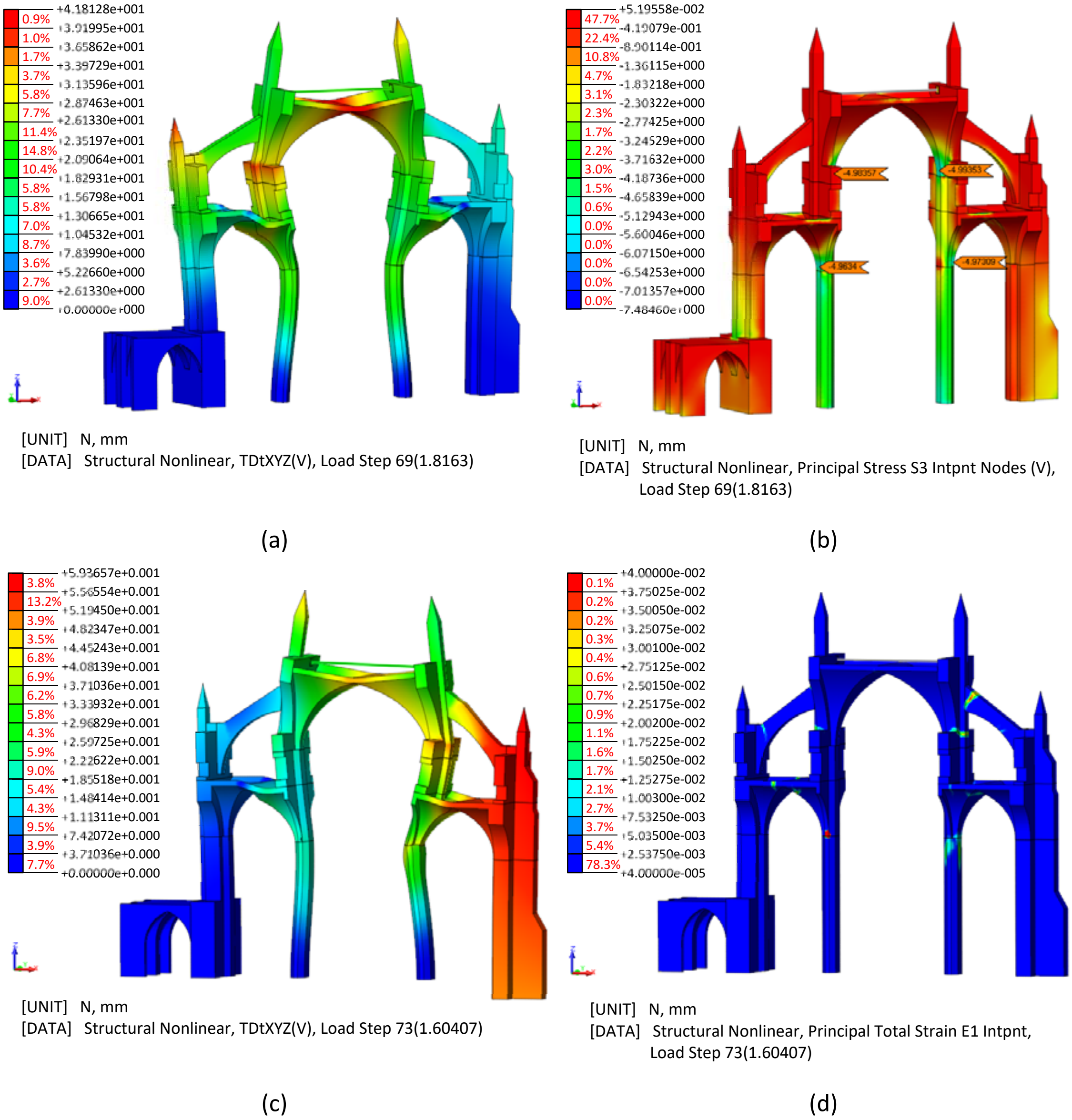

Figure 24. Deformed shape (x100) with incremental displacements (a) and distribution of maximum principal compressive stresses (b) , at a corresponding load step of 1.80g of gravity loading; deformed shape (x100) with incremental displacements (c) and distribution of maximum principal strains (d), at a corresponding load step of 1.60g of gravitational loading and settlements.

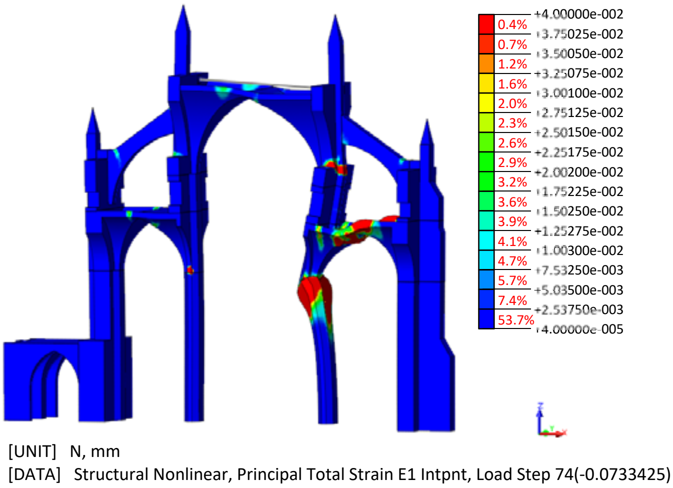

Figure 25. Distribution of maximum principal strains at last load step before failure, under vertical loading and settlement.

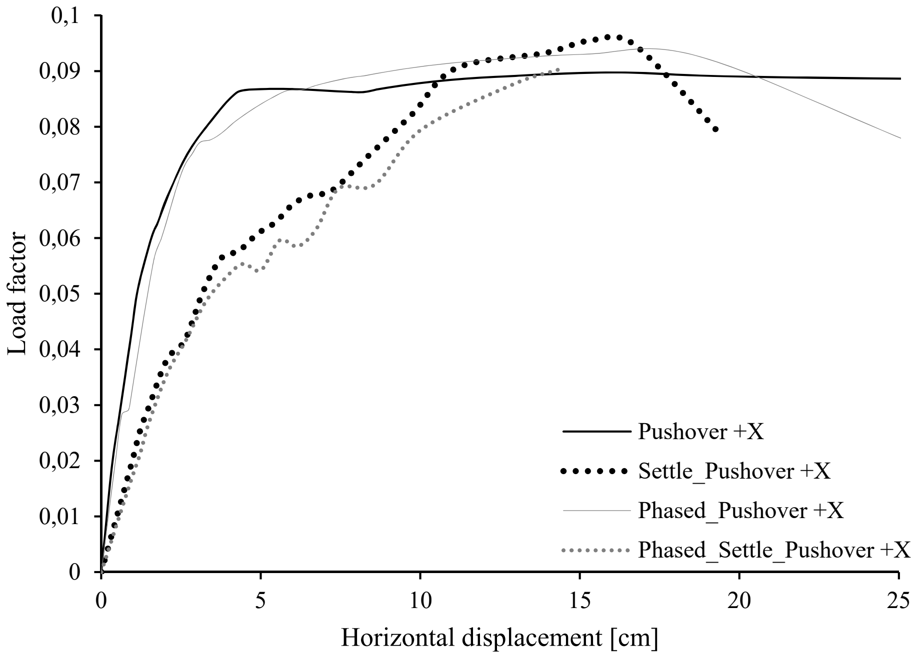

Figure 26. Load displacement diagram, depicting the lateral capacity in terms of horizontal displacements of the nave crown: 1) pushover in lateral direction (Pushover+X); 2) case 1) with settlements (Settle_ Pushover+X); 3) phased analysis followed by pushover in lateral direction (Phased_ Pushover+X); and 4) case 3) with settlements (Phased_Settle _ Pushover+X).

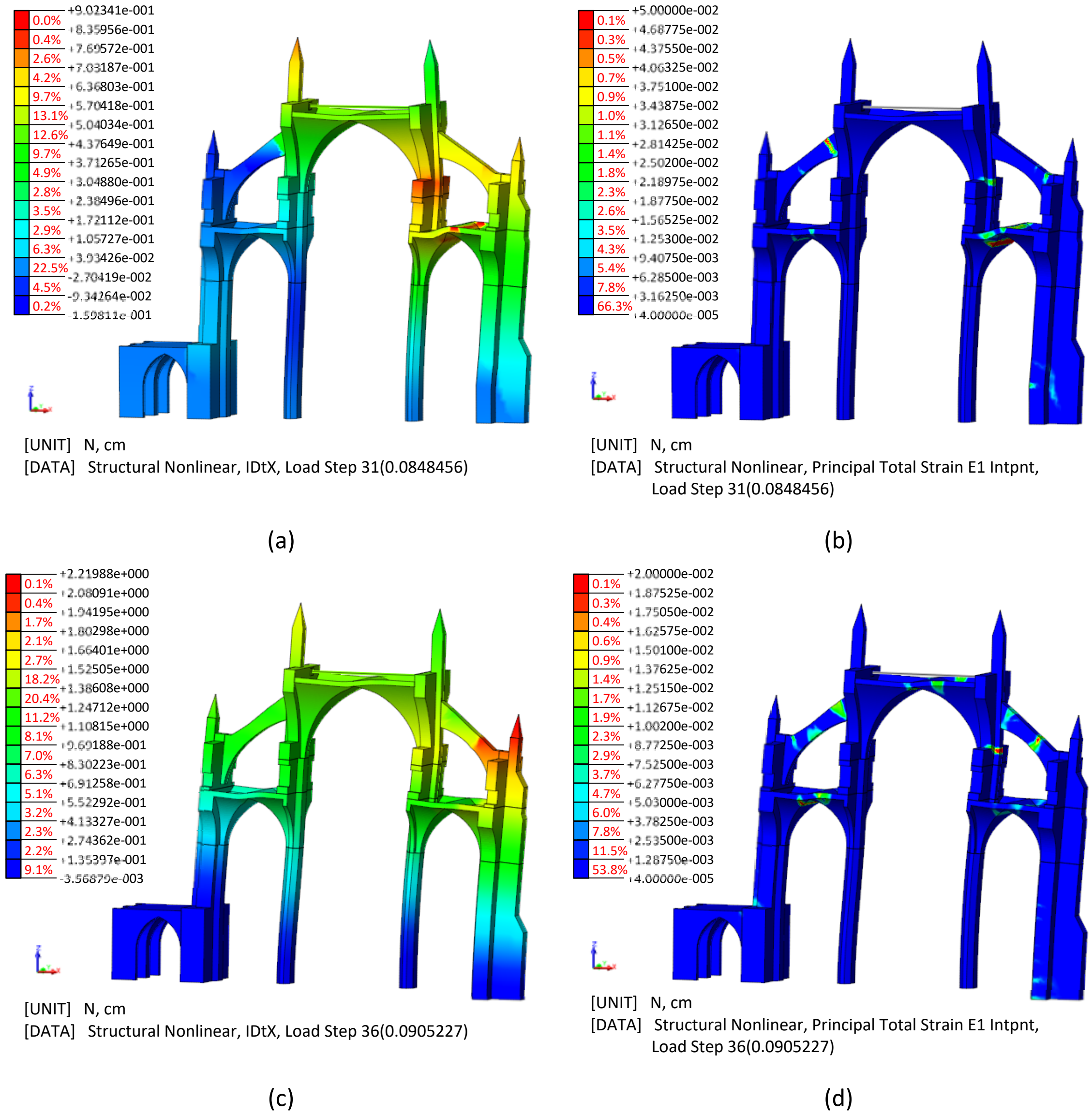

Figure 27. (a) Deformed shape (x100) with incremental displacements, at a corresponding load step of 0.08g of lateral force, under dead loading, (b) distribution of maximum principal strains, at a corresponding load step of 0.08g of lateral force, under dead loading, (c) deformed shape (x100) with incremental displacements, at a corresponding load step of 0.09g of lateral force, under dead loading and settlement, (b) distribution of maximum principal strains, at a corresponding load step of 0.09g of lateral force, under dead loading and settlement.

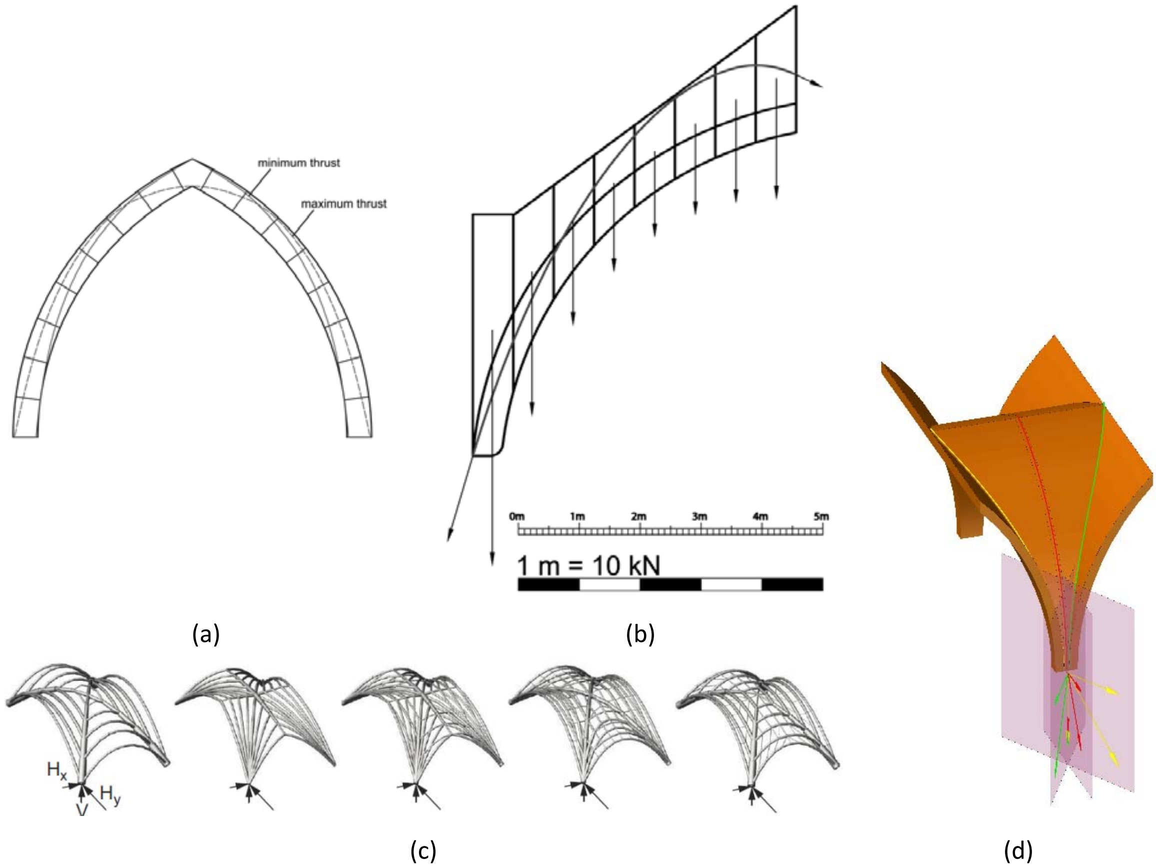

Figure 28. (a) The minimum and maximum thrust line that defines the boundaries of the stability of a pointed Gothic arch, (b) line of thrust in flying buttress of the south aisle in corresponding bay 3, (c) Thrust trajectories in cross vaults in three dimensional view, targeting the springings with different configurations, (d) schematic representation of the resultant thrust in the springing of a Gothic cross vault.

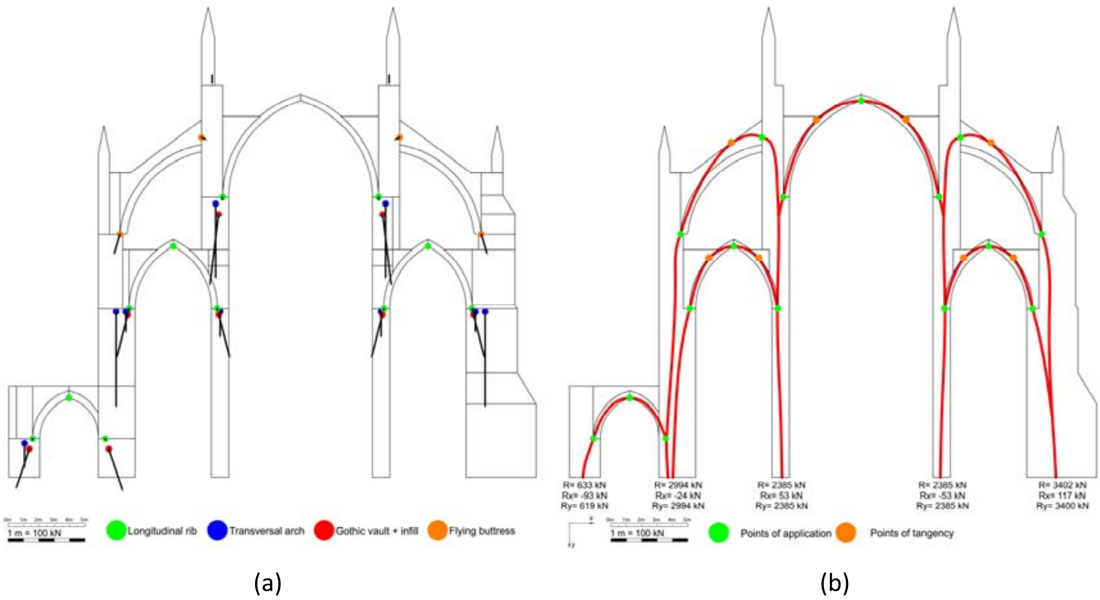

Figure 29. (a) Cross section of the typical bay in macro blocks and the points of application of each force vector of the transversal structural elements, (b) section of the typical bay depicting the line of thrust and the potential hinges, where the thrust line is tangent to the boundaries of the structural elements.

List of Figures